JEM Journal of Experimental Medicine

BRIEF DEFINITIVE REPORT

Altered X-chromosome inactivation of the TLR7/8 locus and heterogeneity of pDCs in systemic sclerosis

Yong Du[1,2*], Bérénice Faz-Lopez[3*], Marie Dominique Ah Kioon[1], Claire Cenac[3], Michael Pierides[1], Kimberly S. Lakin[4], Robert F. Spiera[4], Julie Chaumeil[5], Marie-Elise Truchetet[6,7], Jessica K. Gordon[4], Jean-Charles Guéry[3**], and Franck J. Barrat[1,2**]

Systemic sclerosis (SSc) is an autoimmune disease that has a strong female predominance. Both the X-linked *TLR7* and *TLR8* can induce type I IFN (IFN-I) by plasmacytoid DCs (pDCs), which can promote fibrosis. We identified five subclusters of pDCs, including ISG^{high} clusters that were over-represented in SSc patients. We observed that both *TLR7* and *TLR8* genes escape from X chromosome inactivation (XCI) at higher frequency in pDCs of SSc patients, which was associated with changes in TLR7 protein profile. Combined DNA/RNA FISH analysis revealed that the *TLR7/8* locus is preferentially located outside of the inactive X (Xi) territory when *TLR7* is expressed, suggesting that higher-order loop formation is linked to *TLR7/8* expression from the Xi. Furthermore, the expression levels of *XIST* and the transcriptional repressor *SPEN* were reduced in SSc pDCs. Hence, our data revealed the heterogeneity of pDCs in SSc and suggested that altered XCI at the *TLR7/8* locus may contribute to the chronic IFN-I activity of pDCs in female SSc patients.

Introduction

Systemic sclerosis (SSc) is a disease characterized by elevated autoantibody production, vasculopathy, and fibrosis of the skin and internal organs, and SSc has the highest mortality among autoimmune rheumatic diseases (Allanore et al., 2015; Denton and Khanna, 2017; Hao et al., 2017; Poudel et al., 2018). Serum autoantibodies are present in >95% of patients including autoantibodies specific for nucleic acid (NA)-associated autoantigens, such as anti-topoisomerase 1, anti-centromere, and anti-RNA polymerase III (Allanore et al., 2015; Denton and Khanna, 2017; Kayser and Fritzler, 2015; Poudel et al., 2018; Yang et al., 2020).

There is increasing evidence that the chronic presence of type 1 IFN (IFN-I) responses in both circulation and also in tissues such as the skin and lungs are involved in the pathogenesis of SSc (Ah Kioon et al., 2024; Assassi et al., 2015; Brkic et al., 2016; Christmann et al., 2014; Ciechomska and Skalska, 2018; Crow et al., 2019; Farina et al., 2010; Gardner et al., 2006; Higgs et al., 2011; Johnson et al., 2015; Psarras et al., 2017; Skaug and Assassi, 2019). Further, polymorphisms of IFN regulatory genes (e.g., IRF-4, 5, 7, and 8 and STAT4) are associated with SSc (Skaug and Assassi, 2019), suggesting that IFN-I plays a key role in SSc pathogenesis. We and others have reported that plasmacytoid dendritic cells (pDCs) are key players in the IFN-I response in SSc patients (Ah Kioon et al., 2018; Gerber et al., 2013; van Bon et al., 2014) and can contribute to the establishment and maintenance of skin fibrosis (Ah Kioon et al., 2018). It is likely that the chemokine CXCL4, which was found elevated in the circulation of SSc patients (Lande et al., 2019; van Bon et al., 2014; Volkmann et al., 2016), as well as other chemokines (Du et al., 2022), play a role in promoting the IFN-I response in patients. We and others have also shown that the number of pDCs is decreased in the circulation in SSc patients but infiltrates fibrotic skin (Ah Kioon et al., 2018; Gur et al., 2022) and that the chronic activation of pDCs from patients with SSc is linked to the dysregulation of their metabolic state (Chaudhary et al., 2022). TLR8, which is normally highly expressed on myeloid cells but not on pDCs, is ectopically expressed on pDCs of SSc patients and induces IFN-α in response to a specific agonist

[1]HSS Research Institute and David Z. Rosensweig Genomics Research Center, Inflammation and Autoimmunity Program, Hospital for Special Surgery, New York, NY, USA; [2]Department of Microbiology and Immunology, Weill Cornell Medical College of Cornell University, New York, NY, USA; [3]Institut Toulousain des Maladies Infectieuses et Inflammatoires, Université de Toulouse, INSERM, CNRS, UPS, Toulouse, France; [4]Division of Rheumatology and Scleroderma and Vasculitis Center, Department of Medicine, Hospital for Special Surgery, New York, NY, USA; [5]Institut Cochin, Université Paris Cité, CNRS, INSERM, Paris, France; [6]ImmunoConcEpt, CNRS, UMR 5164, University of Bordeaux, Talence, France; [7]Rheumatology Department, CHU de Bordeaux, Bordeaux, France.

*Y. Du and B. Faz-Lopez contributed equally to this paper; **J.-C. Guéry and F.J. Barrat contributed equally to this paper. Correspondence to Franck J. Barrat: barratf@hss.edu; Jean-Charles Guéry: jean-charles.guery@inserm.fr.

of TLR8 (Ah Kioon et al., 2018). However, little is known about the heterogeneity of the pDC subsets in patients with SSc, why *TLR8* is expressed and how it signals in pDCs, and whether the female predominance, well-described in SSc, is associated with the chronic activation of these cells in patients.

The regulation of expression of X chromosome–encoded genes is important as it is well documented that, like many other autoimmune diseases, SSc is more prevalent in women (Conrad et al., 2023; Jiwrajka and Anguera, 2022; Libert et al., 2010). In female mammals, one of the two X chromosomes is randomly inactivated to equalize the dosage of gene expression between the biological XX and XY sexes (Lyon, 1961). This chromosome-wide gene silencing is triggered, during early embryonic development, by the *XIST* long-coding RNA, which is overexpressed and decorates the X chromosome chosen to be inactivated (Xi) and recruits many protein partners involved in gene silencing per se (SPEN), or the stable epigenetic maintenance of the inactive state (Dossin et al., 2020; Loda et al., 2022). X chromosome inactivation (XCI) results in cellular mosaicism, where about one-half of the cells in a tissue express the maternal X chromosome and the other half the paternal one. However, 15–23% of human X-linked genes escape XCI and are thus expressed from both the active (Xa) and inactive (Xi) X chromosomes in certain tissues or individuals (Carrel and Willard, 2005; Tukiainen et al., 2017). Of importance for this study, mice that express two copies of the *Tlr7* or *Tlr8* gene, both of which are in the same region on the X chromosome, or the expression of a gain of function mutant of human *TLR7* with enhanced signaling potential, is enough to induce full-blown autoimmunity (Brown et al., 2022; David et al., 2024; Deane et al., 2007; Guiducci et al., 2013; Walsh et al., 2012). Furthermore, gain of function mutants of UNC93B that leads to increased TLR7 and TLR8 activity were recently reported in patients with lupus (Al-Azab et al., 2024; David et al., 2024; Rael et al., 2024). Hence, the importance of tight regulation of *TLR7* and/or *TLR8* expression led to the hypothesis that escape from silencing by incomplete XCI in immune cells from women, may affect TLR7/8 signaling, resulting in spontaneous triggering of harmful autoreactive and inflammatory responses leading to disease.

The data present herein identify subclusters (SCs) of pDCs with high expression of IFN-I stimulated genes (ISGs) as being enriched in patients with SSc. Using RNA fluorescent in situ hybridization (RNA-FISH) on primary pDCs from healthy donors (HDs) as well as from patients with SSc, we observed a dysregulation of XCI maintenance at the X-linked *TLR7/8* locus that is associated with SSc condition. Furthermore, combined DNA/RNA FISH analysis showed a correlation between *TLR7* expression from the Xi and its looping outside of the Xi territory, suggesting an extensive reorganization of the Xi in biallelic cells. Finally, we show that the key players of the initiation of XCI, the *XIST* long non-coding RNA and its protein partner *SPEN*, are downregulated in pDCs of SSc patients. Hence, our data suggest that the escape of XCI of the *TLR7/8* locus could be associated with the female predominance in SSc by lowering the TLR-driven activation threshold of pDCs, leading to the association of unique SCs with increased IFN-I response.

Results and discussion

Distribution of pDCs in patients with SSc versus HDs at the single-cell level

Although the understanding of the transcriptomic landscape at the single-cell level of pDCs from SSc is critical, using unbiased approaches to study rare cell types such as pDCs, which represent <1% of total peripheral blood mononuclear cell (PBMCs), is creating significant challenges. For example, in SSc patients, an extensive single-cell RNA sequencing (scRNA-seq) analysis that sampled 97 SSc patients and 56 controls, both blood and skin, led to the identification of interesting fibroblast subsets but yielded few hundreds pDCs, which does not allow meaningful subclustering analysis (Gur et al., 2022). In other autoimmune disease like systemic lupus erythematosus (SLE), the elegant analysis of 276,000 cells from 33 patients with pediatric SLE and 11 matching HDs allowed the mapping of pDCs in SCs (Nehar-Belaid et al., 2020), but only 655 pDCs were analyzed.

To better understand the diversity of pDCs and how this cell type contributes to the IFN signature and pathogenesis of SSc, we collected PBMC samples from four female patients with diffuse SSc and from four female HDs for scRNA-seq analysis and designed a strategy to enrich our samples with pDCs (Fig. 1 A). First, $CD3^+$ cells were depleted to remove the T cells followed by purification of pDCs ($CD14^-$ $CD123^+$ $BDCA4^+$). pDCs were mixed with the CD3-depleted fraction at a 1:2 ratio, leading to a mix of cells with about 30% pDCs (Fig. 1, A–C). To minimize the batch effect, we used previously frozen PBMCs, which were sorted and analyzed on the same day, yielding 31,375 total cells for scRNA-seq analysis (Fig. 1 C), including 13,661 and 17,714 cells in the HD and SSc groups, respectively (Fig. 1, C and D). This included 9,885 pDCs as well as monocytes, B cells, NK cells, and DC subsets (Fig. 1, B–G). By comparing the cell type composition of the different samples, we observed that conventional DCs were decreased while non-classical $CD16^+$ monocytes were significantly enriched in SSc patients (Fig. 1, E–G). As we manipulated the pDCs, we found no difference in the ratio of this cell type between patients and HDs (Fig. 1, E–G). By conducting differential gene expression analysis in cell types, we observed that the most significant differences between SSc patients and HDs were in the NK cell and pDC subsets (Fig. 1, C, D, and H). There were also notable differences in monocytes, particularly in the $CD16^+$ subset (Fig. 1 H). These data illustrate that an enrichment strategy, which has also been done in other studies (Cheong et al., 2023; Villani et al., 2017), allows the analysis of a significant number of cells, even for rare cell types, without the need of a large set of donors. Although this approach minimized the batch effect, a key issue with scRNA-seq, as all the samples were prepared, sorted, and loaded on 10× the same day, there are limitations of this approach. First, T cells were not analyzed, and cells were sorted before preparing the libraries. Furthermore, although our enrichment strategy allowed us to analyze a fairly large number of pDCs using a small number of patients, a key limitation is that these patients may not necessarily represent the full spectrum of patients with SSc and that patients at different stages of the disease or under different treatment may show different cellular distribution. Adding more patients who

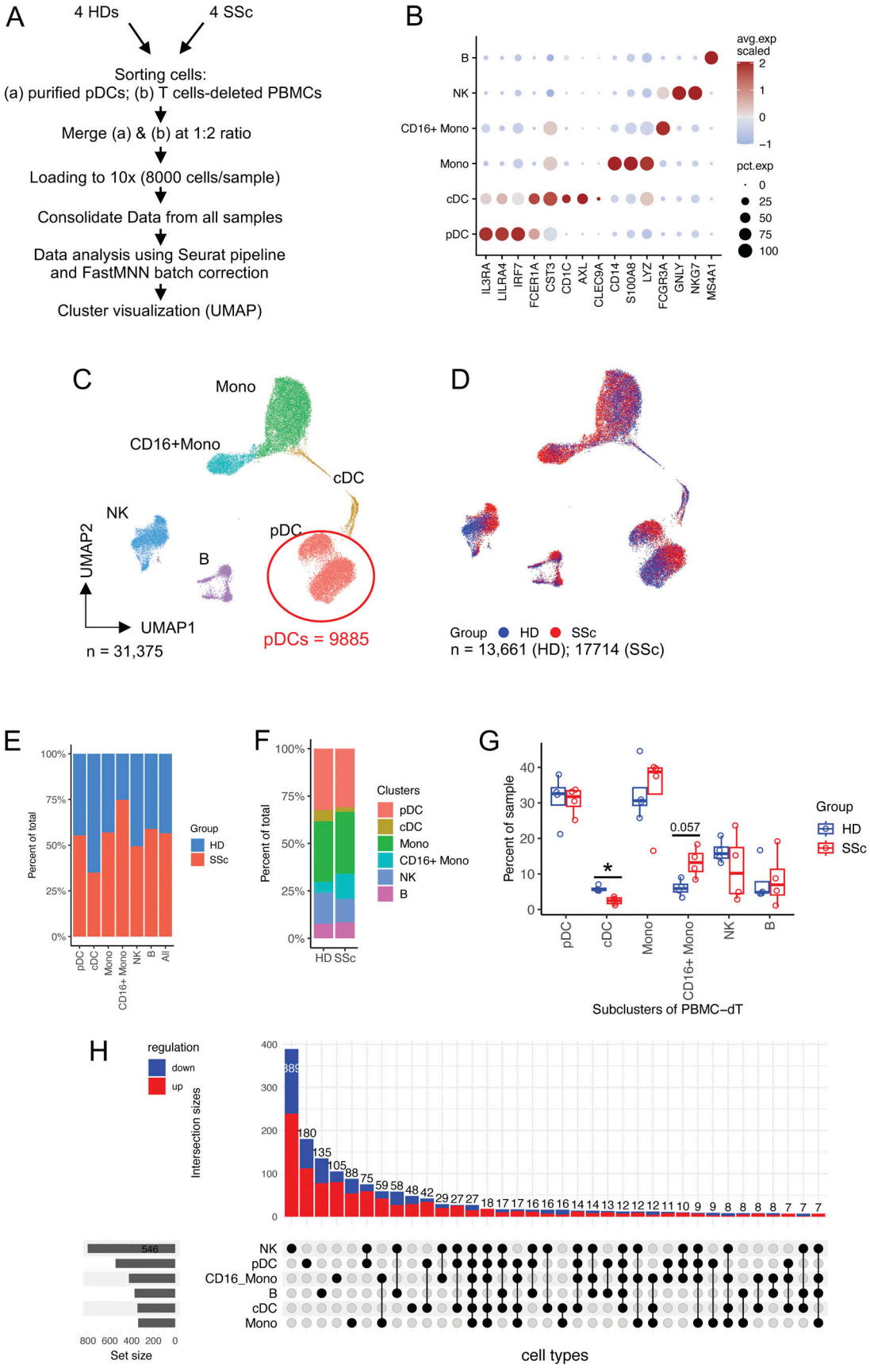

Figure 1. **A pre-enrichment strategy to examine the heterogeneity of pDCs in SSc patients at the single-cell level. (A)** Flow chart describing the sample preparation, library construction, and data processing. Frozen PBMCs from four HDs and four diffuse cutaneous SSc patients were sorted to obtain enriched

pDCs and T cell–depleted PBMCs fractions, the two fractions were then remerged at 1:2 ratio before loading to 10× single-cell microfluidic chips. After library construction and sequencing, a merged dataset with cells was obtained and batch-corrected using FastMNN in a base of Seurat pipeline. Doublets were removed manually, and the data were visualized by UMAP plots. **(B)** Cluster annotation of PBMCs. The dot plot represents expression values of selected genes (x axis) across each cluster (y axis). The color intensity indicates the scaled average expression within expressing cells, where red indicates high expression and blue shows low expression. The dot size represents the percentage of cells expressing the marker genes. **(C)** The UMAP visualization of SCs of merged cells from four healthy and four SSc patients' PBMCs, the putative identity of each cluster was assigned on the basis of B. **(D)** Comparison of the cell distribution of HDs (blue, n = 13,661 cells) and SSc patients (red, n = 17,714 cells) by UMAP plot. **(E)** The ratio of the cell number of healthy donors (n = 4) and SSc patients (n = 4) in each SC is shown by a bar plot. **(F)** Bar plot showing the comparison of the distribution of PBMC SCs between HDs (n = 4) and SSc patients (n = 4). **(G)** Bar plots highlighting cell abundances of different subtypes of PBMCs for healthy donors (n = 4) and SSc patients (n = 4). **(H)** Upset plot showing the intersections of the up-regulated (red, $log_2FC > 0.25$, P_adj < 0.05) and down-regulated (blue, $log_2FC < -0.25$, P_adj < 0.05) in different cell types of PBMCs, Wilcoxon rank sum test was used for DEG identification. Statistical significance in G was evaluated using Mann–Whitney U test, and only comparisons that are significant are shown. *P < 0.05.

receive different treatments should be conducted in further studies.

SCs of cells expressing high levels of IFN-I–inducible genes are enriched in pDCs of SSc patients

To determine the difference between pDCs from patients with SSc versus HDs, we defined the pDC population and conducted SC analysis. We identified five SCs, pDC-0–pDC-4, based on the Uniform Manifold Approximation and Projection (UMAP) plot of the 9,885 pDCs (Fig. 2 A), with the top five expressed marker genes of each SC shown (Fig. 2 B). Of note, we observed cells with a high content of mitochondrial protein-encoding genes such as those described in SLE (Nehar-Belaid et al., 2020), but in our samples, these cells had low mRNA counts, suggesting low viability and hence, were excluded from our analysis. Next, we compared the composition of the clusters between HD and SSc groups. There was a clear imbalance in the distribution of the pDC clusters between SSc patients and HDs, with a larger number of cells from patients in the pDC-0 and pDC-2 SCs and an associated reduction in the SCs pDC-3 and pDC-4, as compared with controls (Fig. 2, C and D). The mapping of ISGs suggested that the pDC-0 and pDC-2 SCs are associated with high IFN-I response (Fig. 2, E and F). Furthermore, pathway analysis based on gene expression of each cluster projected to principal component analysis (PCA) indicated the association of the two SCs with high expression of IFN-I–inducible genes (Fig. S1, A–C and Fig. 2 F). The analysis of the data from each individual donor did not identify that the observed differences between SSc and HDs were due to the dominance of a particular donor, an important control since we used a small number of samples (Fig. S1, D and E). Further, the reactome pathway analysis revealed a chronically activated status of pDCs from SSc patients with multiple inflammatory pathways, including the IFN-I signaling pathway (Fig. S1 B). Using the monocle3 tool (Qiu et al., 2017), we then conducted a trajectory analysis of the different pDC clusters to determine whether the ISG high SCs represented differentiated cells. For this analysis, we selected the ISG^{low} clusters as the starting point and the color and numbers indicate the 10 states identified, with the lower number in the figure indicating the cells that are more undifferentiated when it comes to ISGs, while the higher number stands for the more activated/differentiated cells (Fig. 2 G). The data demonstrate that the pDC-3 and pDC-4 SCs, which are more abundant in HDs, correspond to more resting cells, while the pDC-0 and pDC-2 SCs contained the most activated cells (Fig. 2 H). By separating the HDs and SSc patients' cells, the data show that the activated/differentiated cells are enriched in the patients (Fig. 2, I and J). Interestingly, we also observed that c-Jun and c-Fos, members of activator protein 1 (AP-1) transcription factor family, were enriched in the pDC-3 and pDC-4 SC (Fig. S1 F), and that their expression was reduced in pDCs from SSc patients, which was the opposite for ISGs (Fig. S1 H). Indeed, the AP-1 genes inversely correlated with ISGs expression in the pDCs of SSc patient (Fig. S1 H). Of note, because there is little expression of ISGs in pDCs from HDs, we could not conclude that such correlation exists in pDCs from HDs. Although not much is known about AP-1 function in pDCs beside their contribution to TLR9 signaling in mouse pDCs (Mann-Nüttel et al., 2021), the opposite role between IFN and JUN has been shown in SLE with the ability by IFN-I to downregulate JUN expression (Law et al., 2024). In addition, we observed that chemokine receptors such as CCR2, CCR7, and CXCR3, which are known to be important for pDC migration from blood to tissues (Liu et al., 2021), are significantly upregulated in pDCs of SSc patients (Fig. S1 I) and have higher expression in cells from the ISG^{high} pDC clusters (Fig. S1 J), again suggesting that cells with a more activated/differentiated phenotype are over-represented in patients with SSc. Other studies have described subsets of pDCs in health and disease, including cells that express CD2, which are primarily involved in antigen presentation (Matsui et al., 2009), or where different subsets of pDCs can be induced following their stimulation in vitro (Alculumbre et al., 2018; Duramad et al., 2003), and our data now provide a description of the heterogeneity of pDCs in patients with SSc.

Taken altogether, these data demonstrate a significant unbalance in the activation status of pDCs in patients with SSc as compared with HDs. It also reinforces our understanding of the central role played by IFN-I in pDC-driven activation in SSc.

Dysregulation of the X-linked *TLR7/8* locus in pDCs of women with SSc

There is a clearly increased prevalence in women for multiple autoimmune diseases such as SLE and SSc (Conrad et al., 2023; Jiwrajka and Anguera, 2022; Libert et al., 2010). Notably, it is well documented that increased response to TLR7 or TLR8 is sufficient to induce autoimmunity in mouse models (Christensen et al., 2006; Deane et al., 2007; Guiducci et al., 2013; Pisitkun et al., 2006; Subramanian et al., 2006) or in

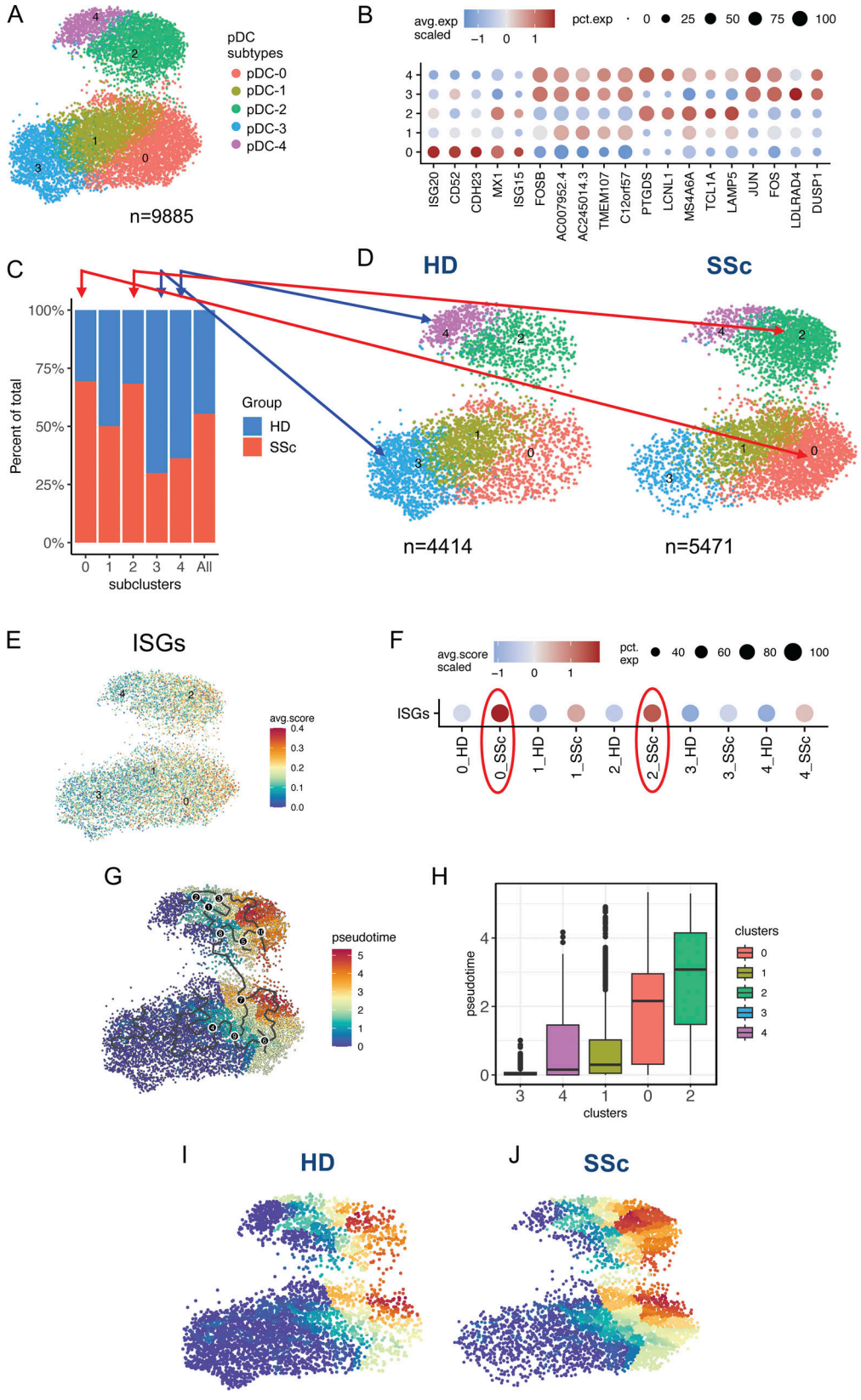

Figure 2. **Enrichment in pDC subsets with high IFN-I signature in SSc patients. (A)** UMAP plots of five SCs of pDCs (n = 9,885 cells). **(B)** A heat map representing scaled expression values of the top five genes defining each SC of pDCs. **(C)** Bar plots highlighting the percentage of the cell number of HDs and SSc patients in each SC of pDCs. **(D)** UMAP plots of SCs of pDCs split by healthy (n = 4,414 cells) and SSc donors (n = 5,471 cells). **(E)** UMAP plot showing the ISGs score in pDCs. **(F)** The comparison of ISGs score of each SC of pDCs. **(G and H)** The trajectory analysis of pDCs. **(I and J)** The UMAP plot shows the trajectory of the pseudotime score in the pDCs of healthy donors and SSc patients, as indicated.

human patients (Al-Azab et al., 2024; Brown et al., 2022; David et al., 2024; Rael et al., 2024). We also reported that *TLR7* and *TLR8* can escape X-chromosome inactivation in immune cells, which is one hypothesis to explain the enhanced prevalence of autoimmunity in female patients and XXY Klinefelter syndrome males (Souyris et al., 2018; Youness et al., 2023). Hence, we next investigated whether aberrant expression of the *TLR7/8* locus from the Xi may occur in primary pDCs from SSc patients. pDCs were isolated from pooled PBMCs from female HDs or SSc patients and then immediately fixed on glass slides. We used RNA FISH probes to detect *TLR7* and *TLR8* primary transcripts together with probes specific for the long non-coding *XIST* RNA, which decorates the Xi territory (Souyris et al., 2018; Youness et al., 2023). Using this approach, we could identify primary pDCs with monoallelic or biallelic expression of either *TLR7* or *TLR8* primary transcripts (Fig. 3, A and B). The proportion of pDCs showing one or two *TLR7* (Fig. 3 C) or *TLR8* (Fig. 3 D) RNA signals was significantly higher in pDCs from the SSc women groups than among age-matched healthy controls, whereas nuclei with robust *XIST* RNA cloud on the Xi territory were relatively infrequent (Fig. S2, A and B). We selected to pool donors due to the need for a high number of cells to conduct RNA FISH, which is a limitation in this study. We then calculated the percentage for each *XIST* RNA localization pattern (types I–IV, previously described in Syrett et al. [2017], Wang et al. [2016]), and we observed that most of the pDCs (>70%) from HD and SSc female donors exhibited Type-III and -IV patterns and therefore lacked robust *XIST* RNA clouds (Fig. S2, A and B). Although the proportion of cells harboring more robust *XIST* RNA clouds (i.e., Type I–Type II patterns) was very heterogeneous among donors, ranging from 3% to 30%, this population of cells tended to be more frequent in SSc pDCs compared with HDs (Fig. S2 C). Then, we calculated the proportion of cells with a biallelic expression of *TLR7* among all *TLR7*$^+$ nuclei (mono + biallelic) in both HD and SSc donors and found that they were homogeneous within the two categories of donors (Fig. 3 E). Strikingly, *TLR7* biallelic cell frequencies were higher in SSc pDCs, reaching 30–40% of total *TLR7*$^+$ pDCs, compared with 10–20% in HDs in the four independent experimental pools tested (Fig. 3, E and F). Similar results were found when nuclei with robust XIST$^+$ Type-I and -II patterns were excluded (Fig. S2 D). Because of the low frequency of nuclei positive for *TLR8* RNA FISH signals, in particular in the HD pools (Fig. 3 B), this analysis could not be performed. However, by combining the four pools of HDs' cells and the ones of female SSc patients' cells, we observed a slight increase in biallelic expression of *TLR8* in total *TLR8*$^+$ SSc pDC nuclei (12%) compared with HDs (7%), although not significant (Fig. 3 F). This tendency follows the very significant increase in *TLR7* biallelic nuclei in pDCs from patients with SSc (35%), as compared with control HDs (13%) (Fig. 3 F). We next investigated *TLR7* mRNA expression in single-cell sorted pDCs from SSc and HD women as described (Abbas et al., 2022). We evaluated *TLR7* expression in 732 pDCs from 5 SSc patients and 500 pDCs from 5 HDs analyzed individually (Fig. S2 E). *TLR7* mRNA transcripts were expressed at higher levels in SSc pDCs than in control HD cells, corresponding to a 1.85-fold increase in the median expression value (Fig. 3 G). Because *TLR7* expression can be induced by IFN-β and two clusters with strong ISGs were over-represented in pDCs of SSc patients, we examined the impact of IFN-I signaling on *TLR7* expression in primary HD pDCs. Indeed, incubation of pDCs with IFN-β resulted in a significant upregulation of *TLR7* mRNA expression at single-cell resolution (Fig. 3 H). Moreover, RNA FISH analysis after in vitro culture of primary pDCs with IL-3 (Fig. 3 I) further showed a significant increase in the proportion of cells expressing *TLR7* in the presence of IFN-β (Fig. 3 J). We observed that IFN-β stimulation not only increases the proportion of nuclei expressing *TLR7* primary transcripts (Fig. 3 J) but also the relative proportion of cells with biallelic expression of *TLR7* within the TLR7$^+$ cells (mono + biallelic) (Fig. S2, F and G). Of note, IL-3–mediated pDC maintenance in this system was associated with strong upregulation of XIST$^+$ Type-II clouds (Fig. S2, H and I). By quantifying the effect of IFN-I signaling on *XIST* cloud formation using machine learning approaches, we observed a significant reduction in robust *XIST* cloud Type I–II (Fig. 3 K), which was associated with a concomitant increase in Type-III *XIST* RNA cloud profiles where *XIST* RNA molecules are less condensed on the Xi territory and can even be delocalized from it, suggesting that *XIST* molecules may be displaced and/or less tightly linked to the Xi territory upon IFN-β stimulation (Fig. S2, H and I; and Fig. 3 K).

We next performed sequential RNA FISH (for *TLR7* primary transcripts and *XIST* RNA) and DNA FISH (for the *TLR7/8* region and X chromosomes) analysis on the same nuclei (n = 109) to assess the 3D localization of the *TLR7/8* genomic region relative to the whole Xa and Xi chromosome territories (Fig. 3, L–N). Representative images are shown for cells with *TLR7* expression from both X chromosomes (biallelic cell; Fig. 3 L) or from only the active one (monoallelic cell; Fig. 3 M). The Euclidean distances of the *TLR7/8* genomic region to the edge of the X chromosome territories were then measured on the DNA FISH 3D stacks using IMARIS software (Fig. 3 N). Images of the same nuclei after RNA and DNA FISH were compared in order to (1) verify that the RNA FISH signals corresponded to the DNA FISH signals, (2) assess which X chromosome was the inactive *XIST*-coated one, and (3) assess the transcriptional status of the two *TLR7* alleles, located on the Xa and Xi (examples in Fig. 3, L and M). The *TLR7/8* region, regardless of *TLR7* expression status and the X of origin, tended to be located inside of the X territory, with a mean distance to the edge of −0.07 µm (95% CI: −0.17 to 0.03 µm) when on the Xi and −0.14 µm (95% CI: −0.07 to −0.21 µm) when on the Xa (Fig. 3 N, "Total" bars). There was also no significant difference in the internal location of the region on the Xa, regardless of *TLR7* expression status (means of −0.14 µm when expressed and −0.12 µm when silenced), consistent with the idea that the active X chromosome is accessible to the transcription machinery (Fig. 3 N, "Xa" bars). Similarly, there was no significant difference in the location inside of the X territory when *TLR7* was not expressed, regardless of the X of origin (means of −0.26 µm when on the Xi and −0.12 µm when on the Xa) (Fig. 3 N, "TLR7$^-$" bars). However, these preferential internal locations of *TLR7/8* regions within the X territory, when *TLR7* is on the Xa or is not expressed from the Xi (i.e., submitted

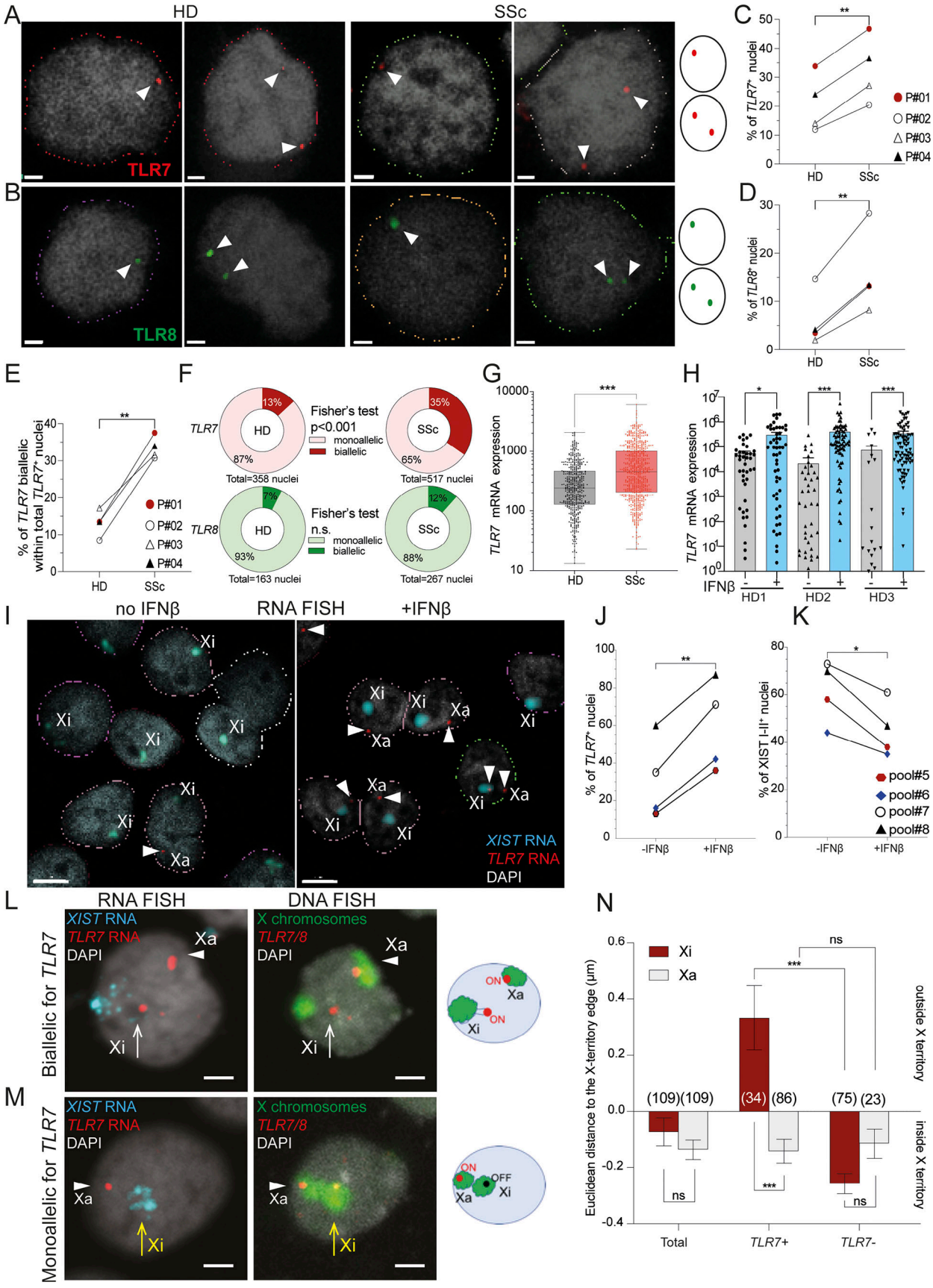

Figure 3. **Evidence for enhanced reactivation of *TLR7* from the inactive X chromosome in pDCs of SSc women. (A and B)** Representative RNA FISH analysis of pDCs from SSc women and HDs. Z-projection of 3D RNA FISH confocal microscopy planes of cell nuclei hybridized with fluorescent probes for

transcripts arising from (A) *TLR7* (red) and (B) *TLR8* (green). Nuclei were counterstained with DAPI (gray). The arrowheads indicate *TLR7* or *TLR8* transcript foci occurring on a single X chromosome (monoallelic cells; left panels) or on both X chromosomes (biallelic cells; right panels). Scale bar, 1 µm. **(C and D)** Quantification of nuclei with one or two RNA FISH signals (mono + biallelic) in pDCs obtained from age-matched control HD (n = 16) and SSc women (n = 21) from four independent experiments (P#01 to P#04); see Table S1. **(E)** Frequency of *TLR7* biallelic nuclei with reference to the total number of positive nuclei (mono + biallelic) in control HD and SSc women from P#01 to P#04 as described in C and D. Statistical differences were analyzed using a paired Student's t test and indicated as **P < 0.01. **(F)** Quantification of allelic expression for *TLR7* and *TLR8* primary transcripts in pooled pDC nuclei from HDs and SSc patients from experiments P#01 to P#04 (C and D). Statistical differences were analyzed using a Fisher's exact test and indicated as *P < 0.05. **(G)** *TLR7* mRNA relative expression from pooled single-cell sorted pDCs from HDs (n = 500 cells, mean cell number/donor = 100, n = 5) and SSc patients (n = 732, mean cell number/donor = 134, n = 5). Statistical analysis was performed using a Mann–Whitney test and indicated as ***P < 0.001. **(H)** pDCs from HDs (n = 3) were single-cell sorted before and after overnight incubation with IFN-β (1 ng/ml) and *TLR7* expression level was quantified by RT-qPCR as described (Abbas et al., 2022). Statistical differences were analyzed using a paired Student's t test and is indicated as *P < 0.05, ***P < 0.001. **(I–K)** pDCs were purified from frozen PBMCs and cultured for 2 days with IL-3 (5 ng/ml) and then incubated with IFN-β (1 ng/ml) for 2 h and processed for RNA FISH analysis with *TLR7* (red) and *XIST* (cyan) specific probes. Representative images showing *TLR7* RNA signals colocalized (expressed from the Xi) or far from the *XIST* cloud (expressed from the Xa), in cells without (left panel) or with IFN-β stimuli (right panel). **(J and K)** (J) Quantification of *TLR7* primary transcripts expression (mono + biallelic cells) and (K) robust *XIST* RNA cloud formation (Types I–II). **(L and M)** Sequential RNA-DNA FISH of *TLR7* expression from the active (Xa) and/or XIST-coated inactive (Xi) chromosomes (RNA FISH) and localization within the X territory (DNA FISH) in female human pDCs. The left panels show single confocal sections of RNA FISH for *TLR7* primary transcripts (red) and *XIST* RNA (cyan) and right panels show DNA FISH for the *TLR7/8* locus (red) and the X chromosomes (green) in the same nuclei. Top row: example of a nucleus with *TLR7* expressed from both the Xa (arrowhead) and *XIST*-coated Xi (white arrow) (biallelic). Bottom row: example of a nucleus with a *TLR7* RNA signal from the Xa (arrowhead) but not from the Xi (yellow arrow) (monoallelic). DAPI is shown in gray. Scale bar = 2 µm. **(N)** Quantification of the Euclidean distance between the *TLR7/8* locus and the edge of the nearest X-chromosome territory. n = 109 XIST+ nuclei across five fields of view with no, mono-, or biallelic expression of *TLR7*. Error bars represent ±SEM, statistical differences between groups were calculated using a one-way ANOVA with Sidack's multiple comparison test. n.s., not significant; *P < 0.05; **P < 0.01; ***P < 0.001.

to XCI), were in striking contrast with the preferential external localization outside of the inactive Xi territory observed when *TLR7* is expressed (i.e., escaping XCI; mean of 0.33 µm [95% CI: 0.10–0.56 µm]) (Fig. 3, L and N "TLR7$^+$" and "Xi" bars). Thus, expression of *TLR7* from the inactive X chromosome (i.e., escape from XCI) correlated with a chromatin looping of the *TLR7/8* genomic region outside the Xi chromosome territory (Fig. 3, L–N). Together, these data suggest that a change in 3D organization of the Xi with the formation of a higher-order loop of the *TLR7/8* region outside of the Xi territory is linked to the escape of *TLR7* from XCI, with the hypothesis that this move could increase the accessibility to the transcription machinery.

Enhanced transcriptional activity of the *TLR7/8* locus translates to TLR8 signaling and dominant expression of the full-length form of the TLR7 protein in pDCs of SSc patients

Our data show increased expression of TLR8 primary transcripts (Fig. 3 D) in pDCs of SSc patients, and we have previously reported that TLR8 is abnormally expressed and IFN-α is produced in response to the specific TLR8 agonist ORN-8L (Ah Kioon et al., 2018) in pDCs of SSc patients. To get a comprehensive view of how these pDCs respond to TLR8 signaling, we performed transcriptomic analysis using RNA-seq of pDCs from four female patients with SSc stimulated by ORN-8L as compared with unstimulated (Unstim). Using PCA, we observed that the TLR8-induced and Unstim conditions differed significantly (Fig. S3 A) and observed a strong induction of IFN-I and IFN-regulated genes as well as the induction of multiple inflammatory cytokines and chemokines upon TLR8 activation (Fig. S3, B–D). Pathway analyses revealed a dominant IFN-I response associated with IRF7 signaling (Fig. S3, E and F), a key transcription factor associated with IFN-I response in pDCs (Guiducci et al., 2008; Honda et al., 2005). Hence, these data suggest that the aberrant presence of TLR8 transcripts in pDCs of SSc patients likely adds another layer of IFN-I induction as compared with a distinct signaling response to the other TLR7&9.

We then examined TLR7 protein levels on FACS-sorted pDCs using a C-terminus TLR7-specific antibody. As we previously reported (Souyris et al., 2018), this antibody can detect both the full-length and the cleaved form of the TLR7 protein (Fig. 4, A–C). We observed that although there was no significant difference in the levels of the full-length form of TLR7 between HDs and SSc patients (Fig. 4, A and B), there was a significant reduction in the cleaved form in SSc patients (Fig. 4, A and C). This led to a significant reduction of the ratio between the cleaved and the full-length forms in SSc pDCs compared to HD age-matched controls (Fig. 4, A and D). These evaluations were done in a limited number of purified pDCs which is a limitation for such assay; however, the ratio "cleaved/full length" was not impacted by the absolute expression levels of TLR7 and the differences consistent across the donors. We then investigated whether the dominance of the full-length TLR7 protein in SSc pDCs could be a consequence of the upregulated expression of *TLR7* mRNA upon IFN-I signaling. We observed in whole PBMCs that IFN-β stimulation, which upregulated *TLR7* and *MxA* gene expression (Fig. S2 J), was associated with a strong increase in both forms of the TLR7 protein (Fig. 4, E–G); however, the effect on the full-length form was more pronounced, and we observed that IFN-β impacted the ratio cleaved/full length by promoting the accumulation of the full-length TLR7 protein over the truncated form (Fig. 4 H). Such enhanced expression of the unprocessed TLR7 protein over the cleaved form in cells incubated with IFN-β was also observed using purified pDCs (Fig. 4, I–L) and associated with an upregulated expression of *TLR7* and *MxA* transcripts (Fig. S2 K). Thus, IFNAR signaling in female pDCs converts their TLR7 protein expression profile toward a predominant expression of the unprocessed form of TLR7 protein, similar to the profile of ex vivo sorted SSc pDCs (Fig. 4, A and D). The source of IFN-I that may be driving this response could be autocrine and could drive increased TLR7 signaling as previously suggested in the case of HDs (Kim et al., 2014), and this is supported by our and others findings that pDCs of patients

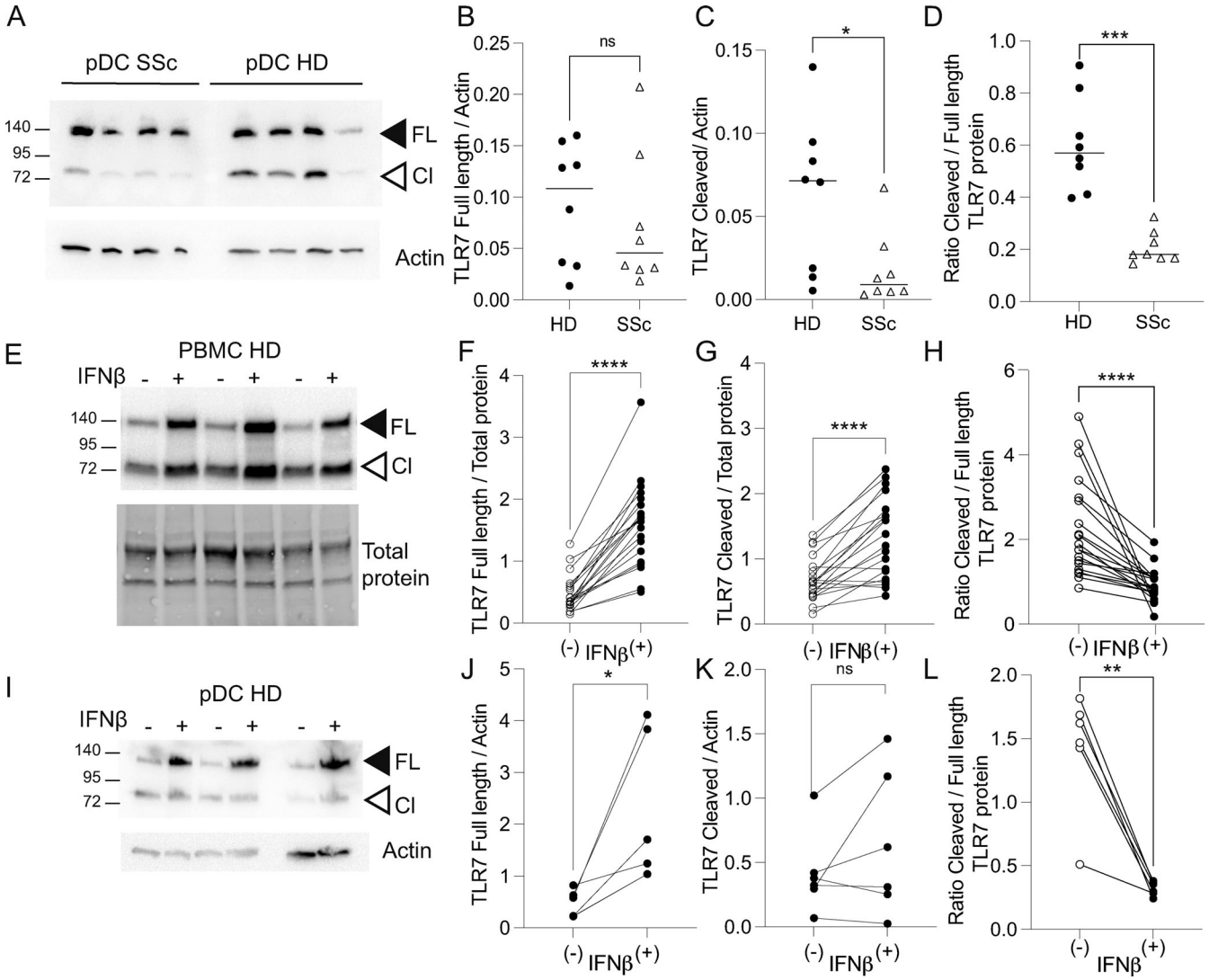

Figure 4. **Levels and distribution of full-length versus cleaved forms of TLR7 protein are altered in pDCs from SSc donors. (A)** Representative western blot of sorted pDCs from SSc patients and HDs. Black arrowhead indicates 140 kDa full-length (FL) TLR7, while white arrowhead indicates the 75 kDa cleaved mature form (Cl). Actin is used as a loading control. **(B and C)** Densitometric analysis of TLR7 full-length and cleaved protein normalized to actin. **(D)** TLR7 proteins expressed as a ratio of TLR7 cleaved over full length from SSc patients (n = 8) and HDs (n = 8) pDCs. Statistical significance was analyzed using Mann–Whitney t test. *P < 0.05; ***P < 0.001. **(E–H)** PBMCs (n = 33) were incubated overnight with 1 ng/ml IFN-β and analyzed for TLR7 expression. **(F and G)** Densitometric analysis of TLR7 full-length and cleaved protein normalized to total protein. TLR7 proteins are expressed as a ratio of TLR7 cleaved over full length. **(I–L)** Sorted pDCs (n = 6) were incubated overnight with 1 ng/ml IFN-β or left untreated and analyzed for TLR7 expression. **(I–K)** Densitometric quantification of TLR7 full length and cleaved protein normalized to actin. **(L)** TLR7 proteins were expressed as a ratio of TLR7 cleaved over full length. **(F–H and J–L)** Statistical significance was analyzed using Wilcoxon paired t test; *P < 0.05, **P < 0.01, ****P < 0.0001. Source data are available for this figure: SourceData F4.

with SSc chronically produce IFN-α, as compared to healthy donors (Ah Kioon et al., 2018; van Bon et al., 2014).

Together, these results show that the observed increase in *TLR7* primary transcripts (Fig. 3, A and C) and higher frequencies of *TLR7* biallelic cells (Fig. 3, E and F) associated with a 1.85-fold upregulation of *TLR7* mRNA at single-cell resolution (Fig. 3 G) are associated with the enhanced expression of full-length TLR7 protein in pDCs of female SSc patients (Fig. 4, A and B). We also observed that these differences are magnified by IFN-β, suggestive of a higher transcriptional activity of *TLR7* loci from both X chromosomes that could be driven by IFN-I signaling.

Reduced expression levels of *XIST* RNA and the transcriptional repressor SPEN, as well as alteration of other histone-modifying enzymes in pDCs of SSc patients

The observation of the presence of IFN-I–associated pDC clusters associated with a defect in XCI at the *TLR7/8* locus in pDCs of SSc patients raised the question as to the mechanism involved which could explain the enrichment during the course of disease of pDCs with such a phenotype.

Xist RNA triggers gene silencing via the recruitment of the transcriptional repressor SPEN (Dossin et al., 2020) and recruits a series of chromatin and epigenetic modifiers resulting in the formation of a heterochromatic Xi compartment with repressive

histone modifications and DNA methylation (Loda et al., 2022). Importantly, reduced *Xist* expression results in overexpression and reactivation of genes on the Xi leading to spontaneous autoimmunity (Huret et al., 2024). The link between a defect in XCI and disease has been suggested both in SLE (Pyfrom et al., 2021), but also in SSc where dysregulated epigenetic factors correlated with the ISG signature in monocytes of SSc patients (van der Kroef et al., 2019). Hence, we compared the expression of *XIST* in pDCs at the single-cell level and observed a reduction in the expression level of *XIST* in SSc patients as compared with HDs (Fig. 5 A). We also observed a reduction of *SPEN* and *CBX4* (Fig. 5 B) and an increase in the expression of *ING4* (Fig. 5 C), which may directly or indirectly enhance permissive H3K27ac deposition as suggested in SSc monocytes (van der Kroef et al., 2019). We then asked whether the changes in expression of these chromatin regulators were linked to the enrichment of ISG^{high} SCs in SSc patients. Although there was no difference in the expression for *XIST* between the ISG^{high} and ISG^{Low} clusters (Fig. 5 D), the expression of both *SPEN* and *CBX4* was reduced in the ISG^{high} SCs as compared with the ISG^{Low} ones, and their expression negatively correlated with the presence of ISGs (Fig. 5, E and F). These data suggest that the enrichment of pDCs with high expression of ISGs, with increased transcriptional levels of *TLR7* and *TLR8*, and with an increased presence of cells with biallelic expression of *TLR7* in patients with SSc is related to the dysregulation of key players of the XCI machinery.

Concluding remarks

There is abundant evidence that difficulties in controlling NA response participate in the development of autoimmune diseases (Ah Kioon et al., 2024), and the contribution by pDCs through the production of IFN-I has been shown in both preclinical models and in clinical trials (Barrat and Su, 2019; Furie et al., 2019; Karnell et al., 2021; Reizis, 2019; Werth et al., 2022). We and others have previously reported that pDCs from patients with SSc are chronically activated, secrete IFN-I and CXCL4, which can promote fibrosis and exacerbate TLR signaling (Ah Kioon et al., 2018; Du et al., 2022; Lande et al., 2019; van Bon et al., 2014), and are perturbed at the metabolic level (Chaudhary et al., 2022).

Our data highlight a fundamental bias toward IFN-I pathway activation by pDCs from SSc patients and identified SCs that are associated with the disease. These SCs appear to result from the maturation of more resting pDC clusters that have low ISGs and increased expression of AP-1 genes. To understand the chronic activation of pDCs and the female predominance in SSc, we rationalized that dysregulation of *TLR7* and *TLR8* due to escape from XCI may be involved. Single-cell resolution analysis of *TLR7* and *TLR8* allelic expression in female pDCs revealed enhanced expression of both TLRs in pDCs of SSc patients and a striking increased frequency of *TLR7* biallelic pDCs in SSc patients. This was associated with higher *TLR7* mRNA and upregulated ISGs in our scRNA-seq data. We cannot exclude that the pDC diversity we observed is generated after innate activation rather than being developmentally determined (Alculumbre et al., 2018). However, it has been shown that female pDC with a biallelic expression of *TLR7* constitutively express higher levels of IFN-I mRNA at steady-state, functionally discriminating them from monoallelic cells (Hagen et al., 2020). Indeed, IFN-I is an important positive regulator of early pDC function through its capacity to act in an autocrine/paracrine manner to drive high levels of production of IFN-I (Kim et al., 2014; Wimmers et al., 2018; Wu et al., 2016), and we observed that IFN-β could induce *TLR7* expression as well as *TLR7* primary transcripts from both Xa and Xi in female pDCs. This suggests that *TLR7* biallelic pDCs are poised for efficient production of IFN-I, which could act in an autocrine/paracrine manner to enhance their TLR responsiveness. Whether TLR7-driven IFN-I production by *TLR7* biallelic pDCs is solely responsible for the increased IFN activity observed not only in pDCs (our study) but also in monocytes (van der Kroef et al., 2019) of SSc patients will warrant further investigation. An alternative hypothesis could be that the accumulation of unprocessed TLR7 as a consequence of enhanced transcriptional activity at both *TLR7* loci due to chronic IFN stimulation may interfere with the TLR7/8 axis leading to enhanced TLR8 signaling in SSc pDCs. This stochiometric changes in full-length TLR7 expression could affect endosomal TLR interactions with chaperones such as UNC93B1, thereby regulating their trafficking/turnover, resulting in upregulated TLR7/8 responses, as recently reported for UNC93B1 variants (Al-Azab et al., 2024; David et al., 2024; Rael et al., 2024).

Aberrant overexpression of ISGs in SSc monocytes has been associated with significant inhibition of the expression of histone-modifying enzymes and partners, including the transcriptional repressor SPEN (van der Kroef et al., 2019). We show that ISG^{high} pDC clusters are upregulated in women with SSc, and this is associated with downregulation of *XIST* and *SPEN* expression at single-cell resolution. Interestingly, recent works indicate that the *XIST*'s SPEN-mediated silencing function is not limited to early development and reactivation of silenced Xi genes or upregulation of partially escaping genes can occur upon *XIST/Xist* loss or downregulation in female immune cells, resulting in atypical memory B cell formation (Yu et al., 2021) or in the spontaneous development of systemic B cell autoimmunity (Huret et al., 2024). Indeed, *XIST* has been shown to be continuously required to maintain the silenced status of the Xi through continuous H3K27 deacetylation at enhancers in B cells (Yu et al., 2021). Moreover, modulation of *Xist* RNA levels in adult tissues was reported to directly regulate the expression of X-linked facultative escapees via direct SPEN-mediated silencing (Hauth et al., 2024, *Preprint*). It is tempting to speculate that the downregulation of *XIST/SPEN* we observed in SSc pDCs accounts for the enhanced proportion of pDCs with a biallelic expression of *TLR7*.

Alteration of chromatin regulators, such as SPEN which recruits and activates HDAC3, has been observed not only in SSc monocytes but also in IFN-stimulated healthy monocytes (van der Kroef et al., 2019). Whether IFN-I signaling may contribute to initiating or sustaining the reactivation of silenced genes from the Xi, through *SPEN/XIST* regulation is currently unknown. Interestingly, we observed that stimulation of pDCs with IFN-I can promote the dynamic egress of *XIST* clouds outside the Xi territories. Moreover, we provide evidence that the *TLR7/8* locus

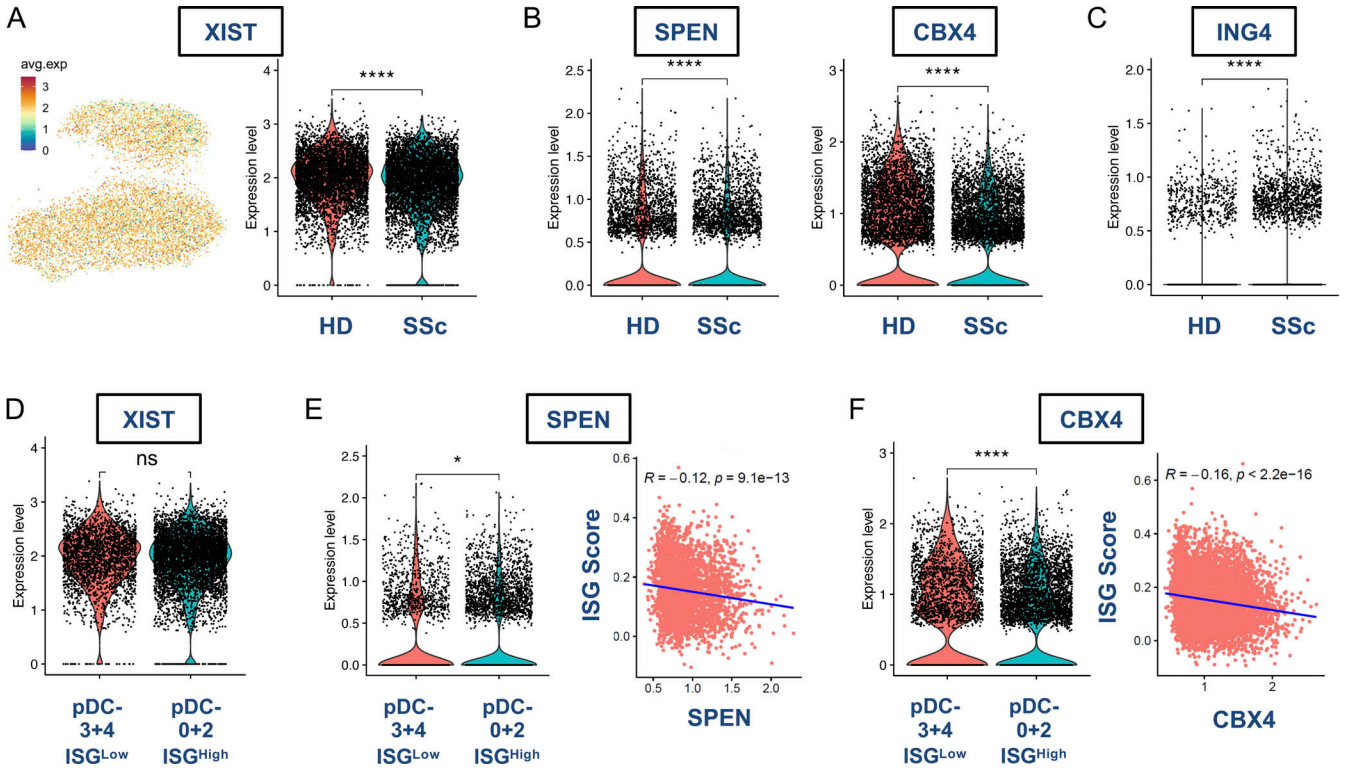

Figure 5. **The expression of X chromosome inactivation-related genes is correlated with ISG score in pDCs of SSc women. (A)** Left: UMAP plot displaying the RNA expression of XIST at the single-cell level in the five SCs of pDCs described in Fig. 2. Right: Violin plot comparing XIST expression between HDs (n = 4) and SSc patients (n = 4). Statistical significance was analyzed using the Wilcoxon rank-sum test and indicated as ****P < 0.0001. **(B and C)** Violin plots illustrating the comparison of (B) SPEN, CBX4, and (C) ING4 expression between HDs and SSc patients are shown. Statistical significance was analyzed using the Wilcoxon rank-sum test and indicated as ****P < 0.0001. **(D)** Violin plot comparing XIST expression between ISG^{low} and ISG^{high} clusters. Statistical significance was analyzed using the Wilcoxon rank-sum test and indicated as ns when non-significant. **(E)** Left: Violin plot comparing SPEN expression between ISG^{low} and ISG^{high} clusters. Right: Correlation analysis between SPEN expression and ISG score. Statistical significance was analyzed using the Wilcoxon rank-sum test and indicated as *P < 0.05. **(F)** Left: Violin plot comparing CBX4 expression between ISG^{low} and ISG^{high} clusters. Right: Correlation analysis between CBX4 expression and ISG score. Statistical significance was analyzed using the Wilcoxon rank-sum test and indicated as ****P < 0.0001. The correlation between ISG score and the expression of the indicated gene was assessed in cells expressing the gene using Pearson correlation, and the corresponding P values were reported.

is often looped out of the Xi territory when *TLR7* is expressed i.e., in the nuclei of *TLR7* biallelic pDCs. These data underline the link between chromatin loop formation and dysregulated expression of the *TLR7/8* locus from the Xi territories in primary pDCs. Such Xi-specific 3D organization of the chromatin may render the *TLR7/8* genes easily accessible to the transcription machinery as previously shown for constitutive escapees in the mouse embryonic stem cell context (Calabrese et al., 2012; Chaumeil et al., 2006; Giorgetti et al., 2016). Whether endogenous IFN-I signaling contributes to the dysregulation of the Xi-linked *TLR7/8* locus in female pDCs through multiple processes, including chromatin modulation, will deserve further investigation.

Thus, pDCs with a high-level expression of *TLR7* mRNA due to the cell-autonomous action of XCI escape of *TLR7* could belong to a group of early responder pDCs with superior ability to produce IFN-I in response to NA sensors such as TLR7, TLR8, and potentially TLR9 signaling, as previously suggested (Wimmers et al., 2018). Such "hyperfunctional" pDCs may accumulate during the course of SSc due to dysregulated epigenetic. Although it is tempting to speculate that the disease-associated pDC SCs in patients with SSc is linked to abnormal XCI maintenance of the X-linked *TLR* locus, cell-extrinsic factors such as inflammatory cytokines or chemokines like CXCL4 and IFN-I signaling, which are likely sustained in SSc patients, could also contribute to their development. While we observed an enhanced proportion of *TLR7* biallelic pDCs in SSc women, which could clearly impact disease progression, our study cannot determine if dysregulated X-linked gene expression causes SSc or is instead a consequence of the disease. Hence, it remains to be determined whether SCs of pDCs, enriched in patients with SSc, correlate with *TLR7* biallelism and are therefore female-specific or whether these ISG^{high} pDC clusters could also emerge from a "XCI escape" independent mechanism in both sexes. Studying pDCs from male patients could also help assess whether pDC heterogeneity is a result of altered XCI and biallelic expression of *TLR7* or dependent on IFN signaling.

In conclusion, by describing the disease-associated pDC SCs in patients with SSc and our observation of dysregulation of XCI maintenance at the X-linked *TLR* locus, our data provide a novel understanding of the pathways associated with disease and the female predominance observed in SSc.

Materials and methods

Reagents and antibodies

The TLR8L agonist ORN-8L (5′-M_2UGCUGCUUGUG-/glycerol/-GUGUUCGUCGUM$_2$-3′) was synthesized by Chemgenes Corporation. The following antibodies were used: APC anti-human CD123(560087; BD), PE anti-human BDCA-4 (130-090-533; Miltenyi), PerCP-Cy5.5 anti-human CD14(562692; BD), and PE-Cy7 anti-human CD3(563423; BD). NEBNext Single Cell/Low Input RNA Library Prep Kit for Illumina (E6420S; NEB) was purchased from New England Biolabs.

Preparation of PBMCs and pDCs

Whole blood or enriched leukocyte buffy coats from healthy donors were obtained from the New York Blood Center (Long Island City, NY, USA) after informed consent of donors who were deemed healthy by the New York Blood Center's criteria. Participants were recruited, and whole blood from SSc patients was collected at the Hospital for Special Surgery, New York, NY, USA, or at the Bordeaux University Hospital, France. All participants provided written informed consent before enrollment. All SSc patients fulfilled the 2013 ACR/EULAR classification criteria for SSc (van den Hoogen et al., 2013). Patients were categorized as having limited cutaneous or diffuse cutaneous subtype of SSc according to LeRoy and Medsger Jr. (LeRoy and Medsger, 2001). Disease duration was defined as the time from the first SSc-related symptom apart from the Raynaud phenomenon. The clinical and demographic characteristics of the SSc patients are described in Table S2 (NY cohort) and Table S3 (France cohort). The blood samples were used under a protocol approved by the Institutional Review Board of the Hospital for Special Surgery and the Institutional Biosafety Committee of Weill Cornell Medicine. PBMCs were prepared using Ficoll–Paque density gradient (GE Healthcare) as previously described (Guiducci et al., 2010). For storage of PBMCs in liquid nitrogen, 10% DMSO + 12.5% human serum albumin in RPMI 1640 or Cryostor (Stemcell) was used for the freezing medium. pDCs were isolated from PBMCs by positive selection using BDCA4-MicroBead Kit as previously described (Guiducci et al., 2010).

scRNA-seq sample preparation, library construction, and data processing

To enrich the PBMCs with pDCs population since the latter are present in the PBMCs in very low frequencies, we first sorted CD3$^+$ cells to remove T cells and then we collected the CD123$^+$BDCA4$^+$CD14$^-$ pDCs and the pDC depleted-PBMC cells (dT&dpDC). We then merged sorted pDCs with the dT&dpDC at a ratio of 1:2 before loading to 10× for scRNA-seq libraries preparation. The cell viability of all donors was above 85%. 8,000 cells from each of the four healthy donors and four SSc patients were loaded onto the same 10× single-cell microfluidic chip to obtain around 5,000 recovery cells. Libraries were constructed by following the company instructions (Chromium Single Cell 3′ Reagent kits v3). The quality of eight libraries was assessed using Agilent Bioanalyzer 2100 and the concentration was quantified by NEBNext Library Quant Kit (E7630S) and equally merged and sequenced by Novaseq. The sequenced data was analyzed in Cellranger to align reads and generate feature-barcode matrices. A merged dataset from four healthy donors and four SSc patients (see Table S4) was batch-corrected and analyzed using FastMNN (Haghverdi et al., 2018) in a R software-based Seurat (Seurat_4.0.3) pipeline (Hao et al., 2021) in SeuratWrappers (https://htmlpreview.github.io/?https://github.com/satijalab/seurat.wrappers/blob/master/docs/fast_mnn.html). Doublets were removed manually by excluding cells with >2 cell type markers. The SCs of the trimmed dataset were visualized by the UMAP plot. The trajectory analysis was performed using the Monocole3 package following the pipeline in SeuratWrappers with minor modification (Qiu et al., 2017), the SC 3 of pDCs was set as the start point.

Differential gene expression and pathway analysis

We used FindMarkers function (logfc.threhold = 0 and min.pct = 0.1) of Seurat with Wilcoxon Rank sum test to obtain a list of differentially expressed genes (DEGs) in each subset of PBMCs. Genes that had Bonferroni corrected P value <0.01, and genes with >0.25 log fold changes were considered significantly different. The pathway analysis of the differentially expressed genes was analyzed by GSEA package (Subramanian et al., 2005) and based on the reactome pathway database. The PCA of pathways of each SC was analyzed by ReactomeGSA package (Griss et al., 2020).

RNA FISH analysis

RNA FISH was performed using established protocols (Chaumeil et al., 2008; Souyris et al., 2018). Probes were prepared by PCR amplification of human genomic DNA fragments using primer sets, targeting exon 1 of XIST (Mendelian inheritance in men [MIM] *314670), and both exon and intron regions of TLR7 (Xp22.2; MIM *300365), TLR8 (Xp22.2; MIM *300366), as described (Youness et al., 2023). Probes were fluorescently labeled using the Vysis Nick Translation kit (Abbott) according to the manufacturer's instructions, and any of the following dUTP conjugates: aminoallyl-dUTP-ATTO-647N, aminoallyl-dUTP-ATTO-550, or aminoallyl-dUTP-XX-ATTO-488 (all from Jena Bioscience). Human pDCs were purified from individual or pooled PBMCs by sequential negative selection with the EasySep human pDC isolation kit (StemCell), followed by FACS-sorting of BDCA4$^+$ CD123$^+$ cells. Purified pDCs were incubated at 37°C for 10 min (10 µl/1–2 × 10^5 cells) on poly-L-lysine–coated coverslips permeabilized for 7 min in ice-cold cytoskeletal buffer containing 0.5% Triton X-100 and 2 mM vanadyl-ribonucleoside complex (New England Biolabs) and immediately fixed for 10 min with 3% paraformaldehyde at room temperature. The cells were dehydrated through successive ethanol baths, air-dried briefly, and incubated with the labeled probes overnight at 42°C. The coverslips were rinsed thrice with 50% formamide in 2× SSC (saline sodium citrate) and thrice with 2× SSC alone, and nuclei were counterstained with DAPI in phosphate-buffered saline. The coverslips were slide-mounted using Dako fluorescence mounting medium before microscopy on a Leica TCS SP8 microscope using a 63× oil immersion objective. Image data were processed with the Fiji software (https://fiji.sc/).

Sequential RNA–DNA FISH

Sequential RNA–DNA FISH was performed in female human pDCs as previously described with minor changes (Chaumeil et al., 2013; Salataj et al., 2023). Briefly, RNA FISH was performed as described in the previous section on cells spotted onto poly-L-lysine–coated glass slides. 3D imaging was performed on a IXplore confocal microscope (Olympus) with a 60× objective and optical sections separated by 0.24 µm, and coordinates of the fields of view were recorded to track the nuclei back after the DNA FISH. To detach the coverslip for the slide and wash off the mounting medium, slides were incubated in three successive baths of 0.2% Tween-20/2× SSC at 42°C. Cells were then predenatured in 0.7% Triton X-100/0.1 M HCl for 10 min on ice and denatured in 50% Formamide/2× SSC for 30 min at 80°C. Cells were then rinsed three times in ice-cold 2× SSC and hybridized with the probes overnight at 42°C. Cells were then washed once in 0.4× SSC for 2 min at 72°C and once in 0.05% Tween-20/2× SSC for 2 min at room temperature. Nuclei were then counterstained with DAPI and mounted with Prolong Gold (Thermo Fisher Scientific) mounting medium. Fields of view imaged after the RNA FISH part were tracked back and imaged again with objective and z-section parameters.

Probe preparation for DNA FISH

The bacterial artificial chromosome (BAC) probe RP11-113P1 for the *TLR7/8* locus was directly labeled by nick translation (kit from Vysis) with aminoallyl-atto-550-dUTP (Jena Bioscience) following the manufacturer's instructions (Vysis). For one slide, 5 µl of the nick translation was precipitated with 1 µg of Cot-1 DNA to anneal all the repetitive sequences potentially present in the BAC. After resuspension in 15 µl of hybridization buffer (50% Formamide, 10% Dextran sulfate, 2× SSC, 2 mg/ml BSA), the probe was denatured at 75°C for 7 min and preannealed for 45 min at 37°C. 5 µl of commercially available green human X chromosome paint (Metasystems) were denatured at 75°C for 5 min and mixed with the *TLR7/8* probe just prior to the hybridization with the cells.

IMARIS analyses

Methodology of machine learning with IMARIS for XIST RNA FISH analyses

Image data were processed with the Fiji software (https://fiji.sc/) and then processed and quantified with the Imaris program version 10.0.1 (Oxford Instrument). Z stack images were taken with a confocal microscope SP8 (Leica microsystems). The same settings were applied for all stacks, then a Z-stack maximum intensity projection was done with the Fiji software. Images were then processed with Imaris software. A background subtraction (mean filtering) was applied according to the area measurements of a few spots, for reference, 1 µm for the red (ATTO-550-TLR7) and green (ATTO-488-TLR8) channel, and 3 µm for cyan (ATTO-647N-XIST). Then a median filter of 3*3*1 for the three channels was done and a Gaussian filter only for XIST of 0.200 µm. Then vectorial isosurfaces were generated around the nucleus (DAPI) with a surface detail of 0.200 µm. Touching nuclei were separated by morphological split. Noncomplete or conglomerates of nuclei were discarded. Nuclei were then classified with machine learning (ML) based on gene expression combinations: one training per gene in combination with XIST was generated (XIST+TLR7, and XIST+TLR8) and one training just for the XIST patterns. The classes were identified as follows for TLR7 and TLR8: XIST/TLR7-8 biallelic, XIST/TLR7-8 in Xa, XIST/TLR7-8 in Xi, XIST, TLR7-8 biallelic, TLR7-8 monoallelic, noXIST/noTLR7-8. For XIST: XIST-I, XIST-II, XIST-III, XIST-IV, and no XIST. For the different trainings, an "Unclassified" class was generated to group all the nuclei that cannot be taken into consideration for the counting, as nuclei with >2 pinpoints, group of nuclei that the program recognized as one, and incomplete nuclei at the border of the field. The program was trained to recognize the spots and clouds according to the color of the channels and the characteristics of the different patterns of XIST of the select nuclei. For that, each class was selected several times among the fields. The results were then validated with manual counting and it showed similar frequencies. Finally, a batch was generated and applied to all images. After each application of the ML system, the data were always revised and the accuracy of the system was confirmed. In a particular case of nuclei in which it was not clear if the nascent signal or TLR7 and TLR8 were from the Xi or Xa were discarded manually.

IMARIS analyses of the distances TLR7-X chromosome territory

Z-stack images were visualized with the Fiji software (https://fiji.sc/). 3D distances between the center of mass of the DNA *TLR7* signals and the edges of their corresponding X chromosome territories were quantified on the DNA FISH z-stacks with the Imaris program using the Cell module (Oxford Instrument). DNA FISH and RNA FISH stacks were then compared to distinguish the inactive XIST-coated and the active X chromosomes.

Western blotting of TLR7 protein

Cell lysates from PBMCs or FACS-sorted pDCs were prepared, quantified, and loaded on precast 4–15% gradient gels (Bio-Rad) as described elsewhere (Azar et al., 2020; Cenac et al., 2022; Souyris et al., 2018). Gels were activated by ultraviolet exposure using a Bio-Rad ChemiDoc MP imager. Proteins were then transferred to Amersham Hybond 0.45-µm polyvinylidene difluoride (PVDF) membranes (GE Healthcare). The membranes were blocked with 5% skim milk and 0.1% Tween-20 in TBS, probed sequentially with anti-human TLR7 (rabbit monoclonal IgG, clone EPR2088[2]; Abcam) antibody overnight, and then with antibodies to β-actin (mouse monoclonal IgG1, clone AC-15; Sigma-Aldrich) 2 h. Bound antibodies were revealed with suitable peroxidase-conjugated secondary antibodies: goat anti-rabbit IgG or horse anti-mouse IgG (Cell Signaling Technology). The membranes were then imaged for Stain-Free staining, and the total protein was quantified using ImageLab 5.0 software (Bio-Rad). Chemiluminescent detection was carried out with Amersham ECL Select or ECL Prime reagents (GE Healthcare). The densitometric signals of the full-length TLR7 145-kDa and the cleaved 75-kDa forms were calculated as described (Cenac et al., 2022).

RNA-seq

Purified pDCs were beads-selected from freshly isolated PBMCs of 40 ml blood collected from four diffuse SSc patients. 1–3 × 10^4

purified pDCs were cultured in 96-U-bottom well with tissue culture medium or TLR8L (ORN-8L) (200 µg/ml) for 6 h. The RNA-based TLR8 agonist, ORN-8L was previously described (Guiducci et al., 2013). Total RNA was isolated using the RNeasy Plus Mini kit. NEBNext Single Cell/Low Input RNA Library Prep Kit for Illumina (E6420S; NEB) was used to prepare Illumina-compatible sequencing libraries. The quality of all RNA was evaluated with BioAnalyser 2100 (Agilent). Pair-end reads were obtained on an Illumina HiSeq 4000 in the Weill Cornell Epigenomics Core Facility at a depth of 16–27 million fragments per sample. Sequencing quality was measured with fastp (Chen et al., 2018). Reads were then mapped in genes counted against the human genome (hg38) with STAR aligner and Gencode v21 (Dobin et al., 2013; Frankish et al., 2019). DEGs expression analysis was performed in R (R Core Team, 2020) using the edgeR package (Robinson et al., 2010). Genes with low expression levels (<3 cpm) were filtered from all downstream analyses. The Benjamini–Hochberg false discovery rate (FDR) procedure was used to calculate the FDR. Genes with FDR <0.05 and $\log_2$ (fold-change) >1 or less than −1 were considered significant.

Single-cell real-time quantitative PCR (RT-qPCR) analysis of TLR7 expression

The workflow for single-cell cDNA analysis described previously has been used in this study (Abbas et al., 2022). Briefly, pDCs from SS or HD women were single-cell-sorted with a FACS Aria-Fusion Cell Sorter (BD Biosciences) in a 96-well plate preloaded with a medium containing 2% Triton X-100, 1 U/µl RNaseOut recombinant ribonuclease inhibitor (Thermo Fisher Scientific), 940 µM dNTPs, and 12.5 ng/µl random hexamer primers (Thermo Fisher Scientific). After cell sorting, single-cell lysates were subjected to RNA reverse transcription using 6.25 U/well Maxima H Minus reverse transcriptase (Thermo Fisher Scientific). Before qPCR, TLR7 were PCR-amplified using TLR7 cDNA-specific primer pairs localized on either side of an intron (P1-exon2, 5′-CTTGGCACCTCTCATGCTCT-3′; P2-exon3 5′-CTG TGCAGTCCACGATCACA-3′), and negative wells screened out by RT-qPCR with nested primers (P2-exon 2, 5′-CTGCTCTCTTCA ACCAGACCT-3′; P3-exon 3, 5′-AAACCATCTAGCCCCAAGGAG-3′) and SsoAdvanced Universal SYBR Green Supermix (Bio-Rad Laboratories). The qPCR was performed using the automated pipetting system epMotion 5070 (Eppendorf) and a Light Cycler 480 instrument (Roche). A limit of detection (LOD) was defined as a Ct value of 23, and then all Ct values higher than the LOD were removed from the analysis. mRNA expression levels were defined as $2^{(\text{LOD-Ct})}$.

Statistical analysis

Data were analyzed using a two-tailed, unpaired Student's *t* test unless specified. Differences were considered significant at a P level <0.05 with *P < 0.05, **P < 0.01, ***P < 0.001.

Online supplemental material

Fig. S1 describes pathways analysis associated with scRNA-seq data. It also shows individual donor analysis and shows differences in the AP-1 transcription factor levels in the different SCs of pDCs. Finally, it shows the distribution of chemokine receptors in the ISG^{high} versus ISG^{low} SCs of pDCs in HD and patients with SSc. Fig. S2 shows the RNA FISH analyses of *XIST* clouds and *TLR7* primary transcript expression in primary pDCs and IL-3–cultured pDCs stimulated or not with IFN-β. It also shows the effect of IFN-I signaling on the dynamic of *XIST* RNA clouds and *TLR7*/*MxA* mRNA expression in PBMCs and pDCs. Fig. S3 shows the RNA-seq analysis of TLR8 signaling in pDCs obtained from patients with SSc. Table S1 shows design of the experimental PBMC pools from SSc and HD tested for pDC enrichment and RNA FISH analysis. Table S2 shows clinical and demographic characteristics of the SSc patients (U.S. cohort). Table S3 shows clinical and demographic characteristics of the SSc patients (France cohort). Table S4 shows clinical and demographic characteristics of the SSc patients used for scRNA-seq analysis.

Data availability

The bulk RNA-seq data assessing the transcriptional effect of TLR8L in SSc pDCs and scRNA-seq data assessing the transcriptional difference of PBMCs between healthy and SSc patients are available in the Gene Expression Omnibus database (accession number GSE210396 and GSE210395, respectively).

Acknowledgments

We thank Dr. Ugur Ayturk at HSS for helping with the 10x library construction as well as Dr. Peggy Crow for the critical reading of the manuscript and the numerous suggestions. We also thank Mia Diaz and Beemnet Amdemicael for providing the clinical information of the patients. We thank Rui Ye from MD Anderson Cancer Center and Steven Zvi Josefowicz from Weill Cornell Medicine for the help of scRNA-seq analysis. We thank the Weill Cornell Epigenomics Core Facility as well as David Oliver for helping with the genomic analysis. We thank Flora Abbas (Institut Toulousain des Maladies Infectieuses et Inflammatoires [INFINITY]) and Delphine Ndiaye-Lobry (Institut Cochin) for their technical assistance. We thank the Imaging Core Facilities of the Institut Cochin (Imag'IC) and INFINITY, Pierre Bourdoncle (Imag'IC), and Sophie Allart (INFINITY) for their help with Imaris analyses.

This work was supported by grants from the National Institutes of Health 1R01AI132447 (F.J. Barrat), the Scleroderma Research Foundation (F.J. Barrat), the Scleroderma Foundation (F.J. Barrat), the FOREUM Foundation for Research in Rheumatology (J.-C. Guéry), and from the Agence Nationale de la Recherche ANR-20-CE15-0014-01 (J.-C. Guéry, J. Chaumeil), ANR-23-CE15-0002-01 (J.-C. Guéry). B. Faz-Lopez was supported by a post-doctoral fellowship from the Inspire Program from Région Occitanie/Pyrénées-Méditerranée (#1901175) and by ANR-23-CE15-0002-01. The David Z. Rosensweig Genomics Center is supported by The Tow Foundation.

Author contributions: Y. Du: Conceptualization, Data curation, Formal analysis, Investigation, Methodology, Validation, Visualization, Writing - original draft, Writing - review & editing, B. Faz-Lopez: Conceptualization, Data curation, Formal analysis, Investigation, Methodology, Software, Validation, M.D.

Ah Kioon: Investigation, Writing - review & editing, C. Cenac: Formal analysis, Investigation, Validation, M. Pierides: Data curation, Investigation, Writing - review & editing, K.S. Lakin: Investigation, Writing - review & editing, R.F. Spiera: Data curation, Investigation, Resources, Writing - review & editing, J. Chaumeil: Conceptualization, Formal analysis, Funding acquisition, Investigation, Methodology, Resources, Validation, Visualization, Writing - review & editing, M.-E. Truchetet: Data curation, Investigation, Resources, Validation, Visualization, Writing - review & editing, J.K. Gordon: Conceptualization, Data curation, Investigation, Project administration, Resources, Supervision, Writing - review & editing, J.-C. Guéry: Conceptualization, Formal analysis, Funding acquisition, Project administration, Resources, Supervision, Validation, Visualization, Writing - original draft, Writing - review & editing, F.J. Barrat: Conceptualization, Funding acquisition, Investigation, Methodology, Project administration, Resources, Supervision, Validation, Visualization, Writing - original draft, Writing - review & editing.

Disclosures: R.F. Spiera reported personal fees from Chemocentryx, AbbVie/Abbott, BMS, Regeneron,Amgen, Vera, GlaxoSmithKline, Novartis, Boehringer Ingelheim, Galderma, Sanofi, Roche Genentech, Cytori, and Astra-Zeneca, and grants from Horizon Pharma, AbbVie/Abbott, AstraZeneca, ChemoCentryx, Corbus, Genentech, GlaxoSmithKline, InflaRx, Kadmon, Novartis, Principia, Roche, Sanofi, Cytori, Boehringer Ingelheim, and Amgen outside the submitted work. M.-E. Truchetet reported personal fees from Abbvie, Boehringer, Janssen, Lilly, and Astrazeneca outside the submitted work. F.J. Barrat reported "other" from Ipinovyx Bio and Epistemyx Bio outside the submitted work. No other disclosures were reported.

Submitted: 4 October 2023
Revised: 26 September 2024
Accepted: 21 November 2024

References

Abbas, F., C. Cenac, A. Youness, P. Azar, P. Delobel, and J.C. Guery. 2022. HIV-1 infection enhances innate function and TLR7 expression in female plasmacytoid dendritic cells. *Life Sci. Alliance*. 5:e202201452. https://doi.org/10.26508/lsa.202201452

Ah Kioon, M.D., P. Laurent, V. Chaudhary, Y. Du, M.K. Crow, and F.J. Barrat. 2024. Modulation of plasmacytoid dendritic cells response in inflammation and autoimmunity. *Immunol. Rev.* 323:241–256. https://doi.org/10.1111/imr.13331

Ah Kioon, M.D., C. Tripodo, D. Fernandez, K.A. Kirou, R.F. Spiera, M.K. Crow, J.K. Gordon, and F.J. Barrat. 2018. Plasmacytoid dendritic cells promote systemic sclerosis with a key role for TLR8. *Sci. Transl. Med.* 10: eaam8458. https://doi.org/10.1126/scitranslmed.aam8458

Al-Azab, M., E. Idiiatullina, Z. Liu, M. Lin, K. Hrovat-Schaale, H. Xian, J. Zhu, M. Yang, B. Lu, Z. Zhao, et al. 2024. Genetic variants in UNC93B1 predispose to childhood-onset systemic lupus erythematosus. *Nat. Immunol.* 25:969–980. https://doi.org/10.1038/s41590-024-01846-5

Alculumbre, S.G., V. Saint-André, J. Di Domizio, P. Vargas, P. Sirven, P. Bost, M. Maurin, P. Maiuri, M. Wery, M.S. Roman, et al. 2018. Diversification of human plasmacytoid predendritic cells in response to a single stimulus. *Nat. Immunol.* 19:63–75. https://doi.org/10.1038/s41590-017-0012-z

Allanore, Y., R. Simms, O. Distler, M. Trojanowska, J. Pope, C.P. Denton, and J. Varga. 2015. Systemic sclerosis. *Nat. Rev. Dis. Primers*. 1:15002. https://doi.org/10.1038/nrdp.2015.2

Assassi, S., W.R. Swindell, M. Wu, F.D. Tan, D. Khanna, D.E. Furst, D.P. Tashkin, R.R. Jahan-Tigh, M.D. Mayes, J.E. Gudjonsson, and J.T. Chang. 2015. Dissecting the heterogeneity of skin gene expression patterns in systemic sclerosis. *Arthritis Rheumatol.* 67:3016–3026. https://doi.org/10.1002/art.39289

Azar, P., J.E. Mejia, C. Cenac, A. Shaiykova, A. Youness, S. Laffont, A. Essat, J. Izopet, C. Passaes, M. Muller-Trutwin, et al. 2020. TLR7 dosage polymorphism shapes interferogenesis and HIV-1 acute viremia in women. *JCI Insight*. 5:e136047. https://doi.org/10.1172/jci.insight.136047

Barrat, F.J., and L. Su. 2019. A pathogenic role of plasmacytoid dendritic cells in autoimmunity and chronic viral infection. *J. Exp. Med.* 216:1974–1985. https://doi.org/10.1084/jem.20181359

Brkic, Z., L. van Bon, M. Cossu, C.G. van Helden-Meeuwsen, M.C. Vonk, H. Knaapen, W. van den Berg, V.A. Dalm, P.L. Van Daele, A. Severino, et al. 2016. The interferon type I signature is present in systemic sclerosis before overt fibrosis and might contribute to its pathogenesis through high BAFF gene expression and high collagen synthesis. *Ann. Rheum. Dis.* 75:1567–1573. https://doi.org/10.1136/annrheumdis-2015-207392

Brown, G.J., P.F. Cañete, H. Wang, A. Medhavy, J. Bones, J.A. Roco, Y. He, Y. Qin, J. Cappello, J.I. Ellyard, et al. 2022. TLR7 gain-of-function genetic variation causes human lupus. *Nature*. 605:349–356. https://doi.org/10.1038/s41586-022-04642-z

Calabrese, G., M. Baldi, D. Fantasia, M.T. Sessa, M. Kalantar, C. Holzhauer, M. Alunni-Fabbroni, G. Palka, and G. Sitar. 2012. Detection of chromosomal aneuploidies in fetal cells isolated from maternal blood using single-chromosome dual-probe FISH analysis. *Clin. Genet.* 82:131–139. https://doi.org/10.1111/j.1399-0004.2011.01775.x

Carrel, L., and H.F. Willard. 2005. X-inactivation profile reveals extensive variability in X-linked gene expression in females. *Nature*. 434: 400–404. https://doi.org/10.1038/nature03479

Cenac, C., M.F. Ducatez, and J.C. Guéry. 2022. Hydroxychloroquine inhibits proteolytic processing of endogenous TLR7 protein in human primary plasmacytoid dendritic cells. *Eur. J. Immunol.* 52:54–61. https://doi.org/10.1002/eji.202149361

Chaudhary, V., M.D. Ah Kioon, S.M. Hwang, B. Mishra, K. Lakin, K.A. Kirou, J. Zhang-Sun, R.L. Wiseman, R.F. Spiera, M.K. Crow, et al. 2022. Chronic activation of pDCs in autoimmunity is linked to dysregulated ER stress and metabolic responses. *J. Exp. Med.* 219:e20221085. https://doi.org/10.1084/jem.20221085

Chaumeil, J., S. Augui, J.C. Chow, and E. Heard. 2008. Combined immunofluorescence, RNA fluorescent in situ hybridization, and DNA fluorescent in situ hybridization to study chromatin changes, transcriptional activity, nuclear organization, and X-chromosome inactivation. *Methods Mol. Biol.* 463:297–308. https://doi.org/10.1007/978-1-59745-406-3_18

Chaumeil, J., P. Le Baccon, A. Wutz, and E. Heard. 2006. A novel role for Xist RNA in the formation of a repressive nuclear compartment into which genes are recruited when silenced. *Genes Dev.* 20:2223–2237. https://doi.org/10.1101/gad.380906

Chaumeil, J., M. Micsinai, P. Ntziachristos, L. Deriano, J.M. Wang, Y. Ji, E.P. Nora, M.J. Rodesch, J.A. Jeddeloh, I. Aifantis, et al. 2013. Higher-order looping and nuclear organization of Tcra facilitate targeted rag cleavage and regulated rearrangement in recombination centers. *Cell Rep.* 3: 359–370. https://doi.org/10.1016/j.celrep.2013.01.024

Chen, S., Y. Zhou, Y. Chen, and J. Gu. 2018. fastp: an ultra-fast all-in-one FASTQ preprocessor. *Bioinformatics*. 34:i884–i890. https://doi.org/10.1093/bioinformatics/bty560

Cheong, J.G., A. Ravishankar, S. Sharma, C.N. Parkhurst, S.A. Grassmann, C.K. Wingert, P. Laurent, S. Ma, L. Paddock, I.C. Miranda, et al. 2023. Epigenetic memory of coronavirus infection in innate immune cells and their progenitors. *Cell*. 186:3882–3902.e24. https://doi.org/10.1016/j.cell.2023.07.019

Christensen, S.R., J. Shupe, K. Nickerson, M. Kashgarian, R.A. Flavell, and M.J. Shlomchik. 2006. Toll-like receptor 7 and TLR9 dictate autoantibody specificity and have opposing inflammatory and regulatory roles in a murine model of lupus. *Immunity*. 25:417–428. https://doi.org/10.1016/j.immuni.2006.07.013

Christmann, R.B., P. Sampaio-Barros, G. Stifano, C.L. Borges, C.R. de Carvalho, R. Kairalla, E.R. Parra, A. Spira, R. Simms, V.L. Capellozzi, and R. Lafyatis. 2014. Association of Interferon- and transforming growth factor β-regulated genes and macrophage activation with systemic sclerosis-related progressive lung fibrosis. *Arthritis Rheumatol.* 66: 714–725. https://doi.org/10.1002/art.38288

Ciechomska, M., and U. Skalska. 2018. Targeting interferons as a strategy for systemic sclerosis treatment. *Immunol. Lett.* 195:45–54. https://doi.org/10.1016/j.imlet.2017.10.011

Conrad, N., S. Misra, J.Y. Verbakel, G. Verbeke, G. Molenberghs, P.N. Taylor, J. Mason, N. Sattar, J.J.V. McMurray, I.B. McInnes, et al. 2023. Incidence, prevalence, and co-occurrence of autoimmune disorders over

time and by age, sex, and socioeconomic status: A population-based cohort study of 22 million individuals in the UK. *Lancet*. 401: 1878–1890. https://doi.org/10.1016/S0140-6736(23)00457-9

Crow, M.K., M. Olferiev, and K.A. Kirou. 2019. Type I interferons in autoimmune disease. *Annu. Rev. Pathol.* 14:369–393. https://doi.org/10.1146/annurev-pathol-020117-043952

David, C., M. Badonyi, R. Kechiche, A. Insalaco, M. Zecca, F. De Benedetti, S. Orcesi, L. Chiapparini, P. Comoli, S. Federici, et al. 2024. Interface gain-of-function mutations in TLR7 cause systemic and neuro-inflammatory disease. *J. Clin. Immunol.* 44:60. https://doi.org/10.1007/s10875-024-01660-6

Deane, J.A., P. Pisitkun, R.S. Barrett, L. Feigenbaum, T. Town, J.M. Ward, R.A. Flavell, and S. Bolland. 2007. Control of toll-like receptor 7 expression is essential to restrict autoimmunity and dendritic cell proliferation. *Immunity*. 27:801–810. https://doi.org/10.1016/j.immuni.2007.09.009

Denton, C.P., and D. Khanna. 2017. Systemic sclerosis. *Lancet*. 390:1685–1699. https://doi.org/10.1016/S0140-6736(17)30933-9

Dobin, A., C.A. Davis, F. Schlesinger, J. Drenkow, C. Zaleski, S. Jha, P. Batut, M. Chaisson, and T.R. Gingeras. 2013. STAR: Ultrafast universal RNA-seq aligner. *Bioinformatics*. 29:15–21. https://doi.org/10.1093/bioinformatics/bts635

Dossin, F., I. Pinheiro, J.J. Żylicz, J. Roensch, S. Collombet, A. Le Saux, T. Chelmicki, M. Attia, V. Kapoor, Y. Zhan, et al. 2020. SPEN integrates transcriptional and epigenetic control of X-inactivation. *Nature*. 578: 455–460. https://doi.org/10.1038/s41586-020-1974-9

Du, Y., M.D. Ah Kioon, P. Laurent, V. Chaudhary, M. Pierides, C. Yang, D. Oliver, L.B. Ivashkiv, and F.J. Barrat. 2022. Chemokines form nanoparticles with DNA and can superinduce TLR-driven immune inflammation. *J. Exp. Med.* 219:e20212142. https://doi.org/10.1084/jem.20212142

Duramad, O., K.L. Fearon, J.H. Chan, H. Kanzler, J.D. Marshall, R.L. Coffman, and F.J. Barrat. 2003. IL-10 regulates plasmacytoid dendritic cell response to CpG-containing immunostimulatory sequences. *Blood*. 102: 4487–4492. https://doi.org/10.1182/blood-2003-07-2465

Farina, G., D. Lafyatis, R. Lemaire, and R. Lafyatis. 2010. A four-gene biomarker predicts skin disease in patients with diffuse cutaneous systemic sclerosis. *Arthritis Rheum.* 62:580–588. https://doi.org/10.1002/art.27220

Frankish, A., M. Diekhans, A.M. Ferreira, R. Johnson, I. Jungreis, J. Loveland, J.M. Mudge, C. Sisu, J. Wright, J. Armstrong, et al. 2019. GENCODE reference annotation for the human and mouse genomes. *Nucleic Acids Res.* 47:D766–D773. https://doi.org/10.1093/nar/gky955

Furie, R., V.P. Werth, J.F. Merola, L. Stevenson, T.L. Reynolds, H. Naik, W. Wang, R. Christmann, A. Gardet, A. Pellerin, et al. 2019. Monoclonal antibody targeting BDCA2 ameliorates skin lesions in systemic lupus erythematosus. *J. Clin. Invest.* 129:1359–1371. https://doi.org/10.1172/JCI124466

Gardner, H., J.R. Shearstone, R. Bandaru, T. Crowell, M. Lynes, M. Trojanowska, J. Pannu, E. Smith, S. Jablonska, M. Blaszczyk, et al. 2006. Gene profiling of scleroderma skin reveals robust signatures of disease that are imperfectly reflected in the transcript profiles of explanted fibroblasts. *Arthritis Rheum.* 54:1961–1973. https://doi.org/10.1002/art.21894

Gerber, E.E., E.M. Gallo, S.C. Fontana, E.C. Davis, F.M. Wigley, D.L. Huso, and H.C. Dietz. 2013. Integrin-modulating therapy prevents fibrosis and autoimmunity in mouse models of scleroderma. *Nature*. 503:126–130. https://doi.org/10.1038/nature12614

Giorgetti, L., B.R. Lajoie, A.C. Carter, M. Attia, Y. Zhan, J. Xu, C.J. Chen, N. Kaplan, H.Y. Chang, E. Heard, and J. Dekker. 2016. Structural organization of the inactive X chromosome in the mouse. *Nature*. 535:575–579. https://doi.org/10.1038/nature18589

Griss, J., G. Viteri, K. Sidiropoulos, V. Nguyen, A. Fabregat, and H. Hermjakob. 2020. ReactomeGSA - efficient multi-omics comparative pathway analysis. *Mol. Cell. Proteomics*. 19:2115–2125. https://doi.org/10.1074/mcp.TIR120.002155

Guiducci, C., C. Ghirelli, M.A. Marloie-Provost, T. Matray, R.L. Coffman, Y.J. Liu, F.J. Barrat, and V. Soumelis. 2008. PI3K is critical for the nuclear translocation of IRF-7 and type I IFN production by human plasmacytoid predendritic cells in response to TLR activation. *J. Exp. Med.* 205: 315–322. https://doi.org/10.1084/jem.20070763

Guiducci, C., M. Gong, A.M. Cepika, Z. Xu, C. Tripodo, L. Bennett, C. Crain, P. Quartier, J.J. Cush, V. Pascual, et al. 2013. RNA recognition by human TLR8 can lead to autoimmune inflammation. *J. Exp. Med.* 210: 2903–2919. https://doi.org/10.1084/jem.20131044

Guiducci, C., M. Gong, Z. Xu, M. Gill, D. Chaussabel, T. Meeker, J.H. Chan, T. Wright, M. Punaro, S. Bolland, et al. 2010. TLR recognition of self nucleic acids hampers glucocorticoid activity in lupus. *Nature*. 465: 937–941. https://doi.org/10.1038/nature09102

Gur, C., S.Y. Wang, F. Sheban, M. Zada, B. Li, F. Kharouf, H. Peleg, S. Aamar, A. Yalin, D. Kirschenbaum, et al. 2022. LGR5 expressing skin fibroblasts define a major cellular hub perturbed in scleroderma. *Cell*. 185: 1373–1388.e20. https://doi.org/10.1016/j.cell.2022.03.011

Hagen, S.H., F. Henseling, J. Hennesen, H. Savel, S. Delahaye, L. Richert, S.M. Ziegler, and M. Altfeld. 2020. Heterogeneous escape from X chromosome inactivation results in sex differences in type I IFN responses at the single human pDC level. *Cell Rep.* 33:108485. https://doi.org/10.1016/j.celrep.2020.108485

Haghverdi, L., A.T.L. Lun, M.D. Morgan, and J.C. Marioni. 2018. Batch effects in single-cell RNA-sequencing data are corrected by matching mutual nearest neighbors. *Nat. Biotechnol.* 36:421–427. https://doi.org/10.1038/nbt.4091

Hao, Y., S. Hao, E. Andersen-Nissen, W.M. Mauck III, S. Zheng, A. Butler, M.J. Lee, A.J. Wilk, C. Darby, M. Zager, et al. 2021. Integrated analysis of multimodal single-cell data. *Cell*. 184:3573–3587.e29. https://doi.org/10.1016/j.cell.2021.04.048

Hao, Y., M. Hudson, M. Baron, P. Carreira, W. Stevens, C. Rabusa, S. Tatibouet, L. Carmona, B.E. Joven, M. Huq, et al. 2017. Early mortality in a multinational systemic sclerosis inception cohort. *Arthritis Rheumatol.* 69:1067–1077. https://doi.org/10.1002/art.40027

Hauth, A., J. Panten, E. Kneuss, C. Picard, N. Servant, I. Rall, Y.A. Perez-Rico, L. Clerquin, N. Servaas, L. Villacorta, et al. 2024. Escape from X inactivation is directly modulated by levels of Xist non-coding RNA. *bioRxiv*. https://doi.org/10.1101/2024.02.22.581559 (Preprint posted February 22, 2024).

Higgs, B.W., Z. Liu, B. White, W. Zhu, W.I. White, C. Morehouse, P. Brohawn, P.A. Kiener, L. Richman, D. Fiorentino, et al. 2011. Patients with systemic lupus erythematosus, myositis, rheumatoid arthritis and scleroderma share activation of a common type I interferon pathway. *Ann. Rheum. Dis.* 70:2029–2036. https://doi.org/10.1136/ard.2011.150326

Honda, K., H. Yanai, H. Negishi, M. Asagiri, M. Sato, T. Mizutani, N. Shimada, Y. Ohba, A. Takaoka, N. Yoshida, and T. Taniguchi. 2005. IRF-7 is the master regulator of type-I interferon-dependent immune responses. *Nature*. 434:772–777. https://doi.org/10.1038/nature03464

Huret, C., L. Ferrayé, A. David, M. Mohamed, N. Valentin, F. Charlotte, M. Savignac, M. Goodhardt, J.C. Guéry, C. Rougeulle, and C. Morey. 2024. Altered X-chromosome inactivation predisposes to autoimmunity. *Sci. Adv.* 10:eadn6537. https://doi.org/10.1126/sciadv.adn6537

Jiwrajka, N., and M.C. Anguera. 2022. The X in seX-biased immunity and autoimmune rheumatic disease. *J. Exp. Med.* 219:e20211487. https://doi.org/10.1084/jem.20211487

Johnson, M.E., J.M. Mahoney, J. Taroni, J.L. Sargent, E. Marmarelis, M.R. Wu, J. Varga, M.E. Hinchcliff, and M.L. Whitfield. 2015. Experimentally-derived fibroblast gene signatures identify molecular pathways associated with distinct subsets of systemic sclerosis patients in three independent cohorts. *PLoS One*. 10:e0114017. https://doi.org/10.1371/journal.pone.0114017

Karnell, J.L., Y. Wu, N. Mittereder, M.A. Smith, M. Gunsior, L. Yan, K.A. Casey, J. Henault, J.M. Riggs, S.M. Nicholson, et al. 2021. Depleting plasmacytoid dendritic cells reduces local type I interferon responses and disease activity in patients with cutaneous lupus. *Sci. Transl. Med.* 13:eabf8442. https://doi.org/10.1126/scitranslmed.abf8442

Kayser, C., and M.J. Fritzler. 2015. Autoantibodies in systemic sclerosis: Unanswered questions. *Front. Immunol.* 6:167. https://doi.org/10.3389/fimmu.2015.00167

Kim, S., V. Kaiser, E. Beier, M. Bechheim, M. Guenthner-Biller, A. Ablasser, M. Berger, S. Endres, G. Hartmann, and V. Hornung. 2014. Self-priming determines high type I IFN production by plasmacytoid dendritic cells. *Eur. J. Immunol.* 44:807–818. https://doi.org/10.1002/eji.201343806

Lande, R., E.Y. Lee, R. Palazzo, B. Marinari, I. Pietraforte, G.S. Santos, Y. Mattenberger, F. Spadaro, K. Stefanantoni, N. Iannace. et al. 2019. CXCL4 assembles DNA into liquid crystalline complexes to amplify TLR9-mediated interferon-alpha production in systemic sclerosis. *Nat. Commun.* 10:1731. https://doi.org/10.1038/s41467-019-09683-z

Law, C., V.S. Wacleche, Y. Cao, A. Pillai, J. Sowerby, B. Hancock, A. Horisberger, S. Bracero, V. Skidanova, Z. Li, et al. 2024. Interferon subverts an AHR-JUN axis to promote CXCL13^{+} T cells in lupus. *Nature*. 631: 857–866. https://doi.org/10.1038/s41586-024-07627-2

LeRoy, E.C., and T.A. Medsger Jr. 2001. Criteria for the classification of early systemic sclerosis. *J. Rheumatol.* 28:1573–1576.

Libert, C., L. Dejager, and I. Pinheiro. 2010. The X chromosome in immune functions: When a chromosome makes the difference. *Nat. Rev. Immunol.* 10:594–604. https://doi.org/10.1038/nri2815

Liu, J., X. Zhang, Y. Cheng, and X. Cao. 2021. Dendritic cell migration in inflammation and immunity. *Cell. Mol. Immunol.* 18:2461–2471. https://doi.org/10.1038/s41423-021-00726-4

Loda, A., S. Collombet, and E. Heard. 2022. Gene regulation in time and space during X-chromosome inactivation. *Nat. Rev. Mol. Cell Biol.* 23:231–249. https://doi.org/10.1038/s41580-021-00438-7

Lyon, M.F. 1961. Gene action in the X-chromosome of the mouse (Mus musculus L.). *Nature*. 190:372–373. https://doi.org/10.1038/190372a0

Mann-Nüttel, R., S. Ali, P. Petzsch, K. Köhrer, J. Alferink, and S. Scheu. 2021. The transcription factor reservoir and chromatin landscape in activated plasmacytoid dendritic cells. *BMC Genom. Data*. 22:37. https://doi.org/10.1186/s12863-021-00991-2

Matsui, T., J.E. Connolly, M. Michnevitz, D. Chaussabel, C.I. Yu, C. Glaser, S. Tindle, M. Pypaert, H. Freitas, B. Piqueras, et al. 2009. CD2 distinguishes two subsets of human plasmacytoid dendritic cells with distinct phenotype and functions. *J. Immunol.* 182:6815–6823. https://doi.org/10.4049/jimmunol.0802008

Nehar-Belaid, D., S. Hong, R. Marches, G. Chen, M. Bolisetty, J. Baisch, L. Walters, M. Punaro, R.J. Rossi, C.H. Chung, et al. 2020. Mapping systemic lupus erythematosus heterogeneity at the single-cell level. *Nat. Immunol.* 21:1094–1106. https://doi.org/10.1038/s41590-020-0743-0

Pisitkun, P., J.A. Deane, M.J. Difilippantonio, T. Tarasenko, A.B. Satterthwaite, and S. Bolland. 2006. Autoreactive B cell responses to RNA-related antigens due to TLR7 gene duplication. *Science*. 312:1669–1672. https://doi.org/10.1126/science.1124978

Poudel, D.R., D. Jayakumar, A. Danve, S.T. Sehra, and C.T. Derk. 2018. Determinants of mortality in systemic sclerosis: A focused review. *Rheumatol. Int.* 38:1847–1858. https://doi.org/10.1007/s00296-017-3826-y

Psarras, A., P. Emery, and E.M. Vital. 2017. Type I interferon-mediated autoimmune diseases: Pathogenesis, diagnosis and targeted therapy. *Rheumatology*. 56:1662–1675. https://doi.org/10.1093/rheumatology/kew431

Pyfrom, S., B. Paneru, J.J. Knox, M.P. Cancro, S. Posso, J.H. Buckner, and M.C. Anguera. 2021. The dynamic epigenetic regulation of the inactive X chromosome in healthy human B cells is dysregulated in lupus patients. *Proc. Natl. Acad. Sci. USA*. 118:e2024624118. https://doi.org/10.1073/pnas.2024624118

Qiu, X., Q. Mao, Y. Tang, L. Wang, R. Chawla, H.A. Pliner, and C. Trapnell. 2017. Reversed graph embedding resolves complex single-cell trajectories. *Nat. Methods*. 14:979–982. https://doi.org/10.1038/nmeth.4402

Rael, V.E., J.A. Yano, J.P. Huizar, L.C. Slayden, M.A. Weiss, E.A. Turcotte, J.M. Terry, W. Zuo, I. Thiffault, T. Pastinen, et al. 2024. Large-scale mutational analysis identifies UNC93B1 variants that drive TLR-mediated autoimmunity in mice and humans. *J. Exp. Med.* 221:e20232005. https://doi.org/10.1084/jem.20232005

Reizis, B. 2019. Plasmacytoid dendritic cells: Development, regulation, and function. *Immunity*. 50:37–50. https://doi.org/10.1016/j.immuni.2018.12.027

Robinson, M.D., D.J. McCarthy, and G.K. Smyth. 2010. edgeR: a Bioconductor package for differential expression analysis of digital gene expression data. *Bioinformatics*. 26:139–140. https://doi.org/10.1093/bioinformatics/btp616

Salataj, E., C.G. Spilianakis, and J. Chaumeil. 2023. Single-cell detection of primary transcripts, their genomic loci and nuclear factors by 3D immuno-RNA/DNA FISH in T cells. *Front. Immunol.* 14:1156077. https://doi.org/10.3389/fimmu.2023.1156077

Skaug, B., and S. Assassi. 2019. Type I interferon dysregulation in systemic sclerosis. *Cytokine*. 132:154635. https://doi.org/10.1016/j.cyto.2018.12.018

Souyris, M., C. Cenac, P. Azar, D. Daviaud, A. Canivet, S. Grunenwald, C. Pienkowski, J. Chaumeil, J.E. Mejia, and J.C. Guery. 2018. TLR7 escapes X chromosome inactivation in immune cells. *Sci. Immunol.* 3:eaap8855. https://doi.org/10.1126/sciimmunol.aap8855

Subramanian, A., P. Tamayo, V.K. Mootha, S. Mukherjee, B.L. Ebert, M.A. Gillette, A. Paulovich, S.L. Pomeroy, T.R. Golub, E.S. Lander, and J.P. Mesirov. 2005. Gene set enrichment analysis: A knowledge-based approach for interpreting genome-wide expression profiles. *Proc. Natl. Acad. Sci. USA*. 102:15545–15550. https://doi.org/10.1073/pnas.0506580102

Subramanian, S., K. Tus, Q.Z. Li, A. Wang, X.H. Tian, J. Zhou, C. Liang, G. Bartov, L.D. McDaniel, X.J. Zhou, et al. 2006. A Tlr7 translocation accelerates systemic autoimmunity in murine lupus. *Proc. Natl. Acad. Sci. USA*. 103:9970–9975. https://doi.org/10.1073/pnas.0603912103

Syrett, C.M., V. Sindhava, S. Hodawadekar, A. Myles, G. Liang, Y. Zhang, S. Nandi, M. Cancro, M. Atchison, and M.C. Anguera. 2017. Loss of Xist RNA from the inactive X during B cell development is restored in a dynamic YY1-dependent two-step process in activated B cells. *PLoS Genet.* 13:e1007050. https://doi.org/10.1371/journal.pgen.1007050

R Core Team. 2020. R: A Language and Environment for Statistical Computing. R Foundation for Statistical Computing, Vienna, Austria. https://www.r-project.org/.

Tukiainen, T., A.C. Villani, A. Yen, M.A. Rivas, J.L. Marshall, R. Satija, M. Aguirre, L. Gauthier, M. Fleharty, A. Kirby, et al. 2017. Landscape of X chromosome inactivation across human tissues. *Nature*. 550:244–248. https://doi.org/10.1038/nature24265

van Bon, L., A.J. Affandi, J. Broen, R.B. Christmann, R.J. Marijnissen, L. Stawski, G.A. Farina, G. Stifano, A.L. Mathes, M. Cossu, et al. 2014. Proteome-wide analysis and CXCL4 as a biomarker in systemic sclerosis. *N. Engl. J. Med.* 370:433–443. https://doi.org/10.1056/NEJMoa1114576

van den Hoogen, F., D. Khanna, J. Fransen, S.R. Johnson, M. Baron, A. Tyndall, M. Matucci-Cerinic, R.P. Naden, T.A. Medsger Jr., P.E. Carreira, et al. 2013. 2013 classification criteria for systemic sclerosis: An American college of Rheumatology/European league against rheumatism collaborative initiative. *Arthritis Rheum.* 65:2737–2747. https://doi.org/10.1002/art.38098

van der Kroef, M., M. Castellucci, M. Mokry, M. Cossu, M. Garonzi, L.M. Bossini-Castillo, E. Chouri, C.G.K. Wichers, L. Beretta, E. Trombetta, et al. 2019. Histone modifications underlie monocyte dysregulation in patients with systemic sclerosis, underlining the treatment potential of epigenetic targeting. *Ann. Rheum. Dis.* 78:529–538. https://doi.org/10.1136/annrheumdis-2018-214295

Villani, A.C., R. Satija, G. Reynolds, S. Sarkizova, K. Shekhar, J. Fletcher, M. Griesbeck, A. Butler, S. Zheng, S. Lazo, et al. 2017. Single-cell RNA-seq reveals new types of human blood dendritic cells, monocytes, and progenitors. *Science*. 356:eaah4573. https://doi.org/10.1126/science.aah4573

Volkmann, E.R., D.P. Tashkin, M.D. Roth, P.J. Clements, D. Khanna, D.E. Furst, M. Mayes, J. Charles, C.H. Tseng, R.M. Elashoff, and S. Assassi. 2016. Changes in plasma CXCL4 levels are associated with improvements in lung function in patients receiving immunosuppressive therapy for systemic sclerosis-related interstitial lung disease. *Arthritis Res. Ther.* 18:305. https://doi.org/10.1186/s13075-016-1203-y

Walsh, E.R., P. Pisitkun, E. Voynova, J.A. Deane, B.L. Scott, R.R. Caspi, and S. Bolland. 2012. Dual signaling by innate and adaptive immune receptors is required for TLR7-induced B-cell-mediated autoimmunity. *Proc. Natl. Acad. Sci. USA*. 109:16276–16281. https://doi.org/10.1073/pnas.1209372109

Wang, J., C.M. Syrett, M.C. Kramer, A. Basu, M.L. Atchison, and M.C. Anguera. 2016. Unusual maintenance of X chromosome inactivation predisposes female lymphocytes for increased expression from the inactive X. *Proc. Natl. Acad. Sci. USA*. 113:E2029–E2038. https://doi.org/10.1073/pnas.1520113113

Werth, V.P., R.A. Furie, J. Romero-Diaz, S. Navarra, K. Kalunian, R.F. van Vollenhoven, F. Nyberg, B.H. Kaffenberger, S.Z. Sheikh, G. Radunovic, et al. 2022. Trial of anti-BDCA2 antibody litifilimab for cutaneous lupus erythematosus. *N. Engl. J. Med.* 387:321–331. https://doi.org/10.1056/NEJMoa2118024

Wimmers, F., N. Subedi, N. van Buuringen, D. Heister, J. Vivié, I. Beeren-Reinieren, R. Woestenenk, H. Dolstra, A. Piruska, J.F.M. Jacobs, et al. 2018. Single-cell analysis reveals that stochasticity and paracrine signaling control interferon-alpha production by plasmacytoid dendritic cells. *Nat. Commun.* 9:3317. https://doi.org/10.1038/s41467-018-05784-3

Wu, D., D.E. Sanin, B. Everts, Q. Chen, J. Qiu, M.D. Buck, A. Patterson, A.M. Smith, C.H. Chang, Z. Liu, et al. 2016. Type 1 interferons induce changes in core metabolism that are critical for immune function. *Immunity*. 44:1325–1336. https://doi.org/10.1016/j.immuni.2016.06.006

Yang, C., S. Tang, D. Zhu, Y. Ding, and J. Qiao. 2020. Classical disease-specific autoantibodies in systemic sclerosis: Clinical features, gene susceptibility, and disease stratification. *Front. Med.* 7:587773. https://doi.org/10.3389/fmed.2020.587773

Youness, A., C. Cenac, B. Faz-López, S. Grunenwald, F.J. Barrat, J. Chaumeil, J.E. Mejía, and J.C. Guéry. 2023. TLR8 escapes X chromosome inactivation in human monocytes and CD4$^+$ T cells. *Biol. Sex Differ.* 14:60. https://doi.org/10.1186/s13293-023-00544-5

Yu, B., Y. Qi, R. Li, Q. Shi, A.T. Satpathy, and H.Y. Chang. 2021. B cell-specific XIST complex enforces X-inactivation and restrains atypical B cells. *Cell*. 184:1790–1803.e17. https://doi.org/10.1016/j.cell.2021.02.015

JEM

Supplemental material

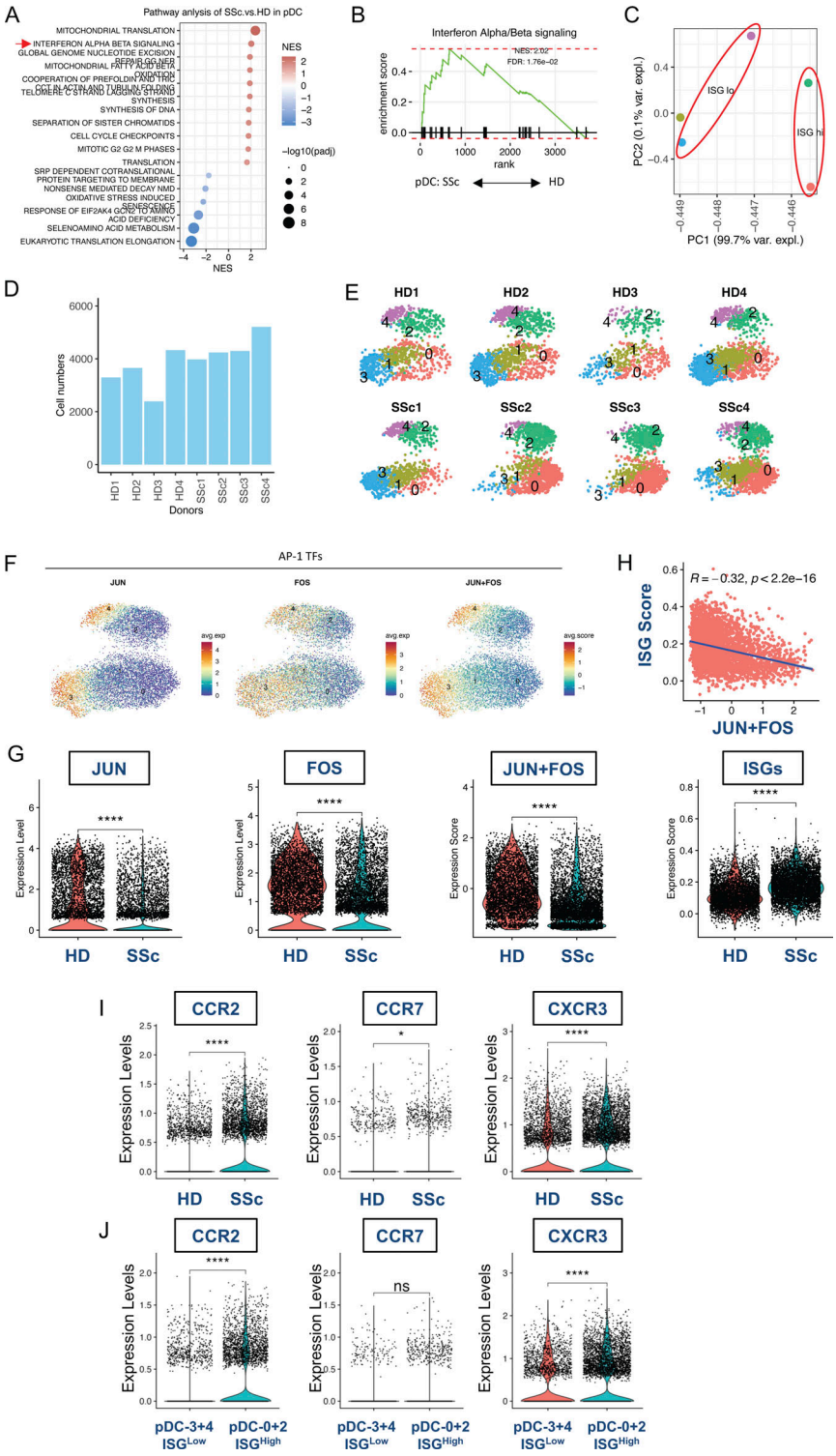

Figure S1. **Description of the pDC SCs in HDs and SSc patients. (A)** Reactome pathway analysis of activated and inactivated pathways in pDCs of SSc patients (n = 4) versus HDs (n = 4). For pathways sharing similar gene sets, only the top first with the highest normalized enriched score (NES) are shown. **(B)** Gene set enrichment analysis of IFN-α/β pathway in SSc versus healthy pDCs. **(C)** PCA of pathways activated in each of the pDC SCs. **(D)** Bar plots highlighting the cell number of the individual HDs (n = 4) and SSc patients (n = 4). **(E)** UMAP plots of the five SCs of pDCs in each of the individual healthy donors (n = 4) and SSc patients (n = 4). **(F)** Feature plot showing the expression of AP-1 transcription factors (JUN, FOS, combined JUN+FOS) in different pDC SCs. **(G)** Violin plot showing the expression of AP-1 transcription factors (JUN, FOS, combined JUN+FOS) and ISGs between HDs and SSc patients. Statistical significance was analyzed using the Wilcoxon rank-sum test; ****P < 0.0001. **(H)** The correlation of expression between AP-1 transcription factors (combined JUN+FOS) with ISGs score in pDCs of SSc patients as assessed using Pearson correlation, and the corresponding P values were reported ($P < 2.2^{e-16}$). **(I and J)** Violin plot showing the expression of CCR2, CCR7 and CXCR3 between (I) HDs and SSc patients and (J) between cells present in the ISG^{low} and ISG^{high} SCs, as indicated. Statistical significance was analyzed using the Wilcoxon rank-sum test and indicated as *P < 0.05, ****P < 0.0001.

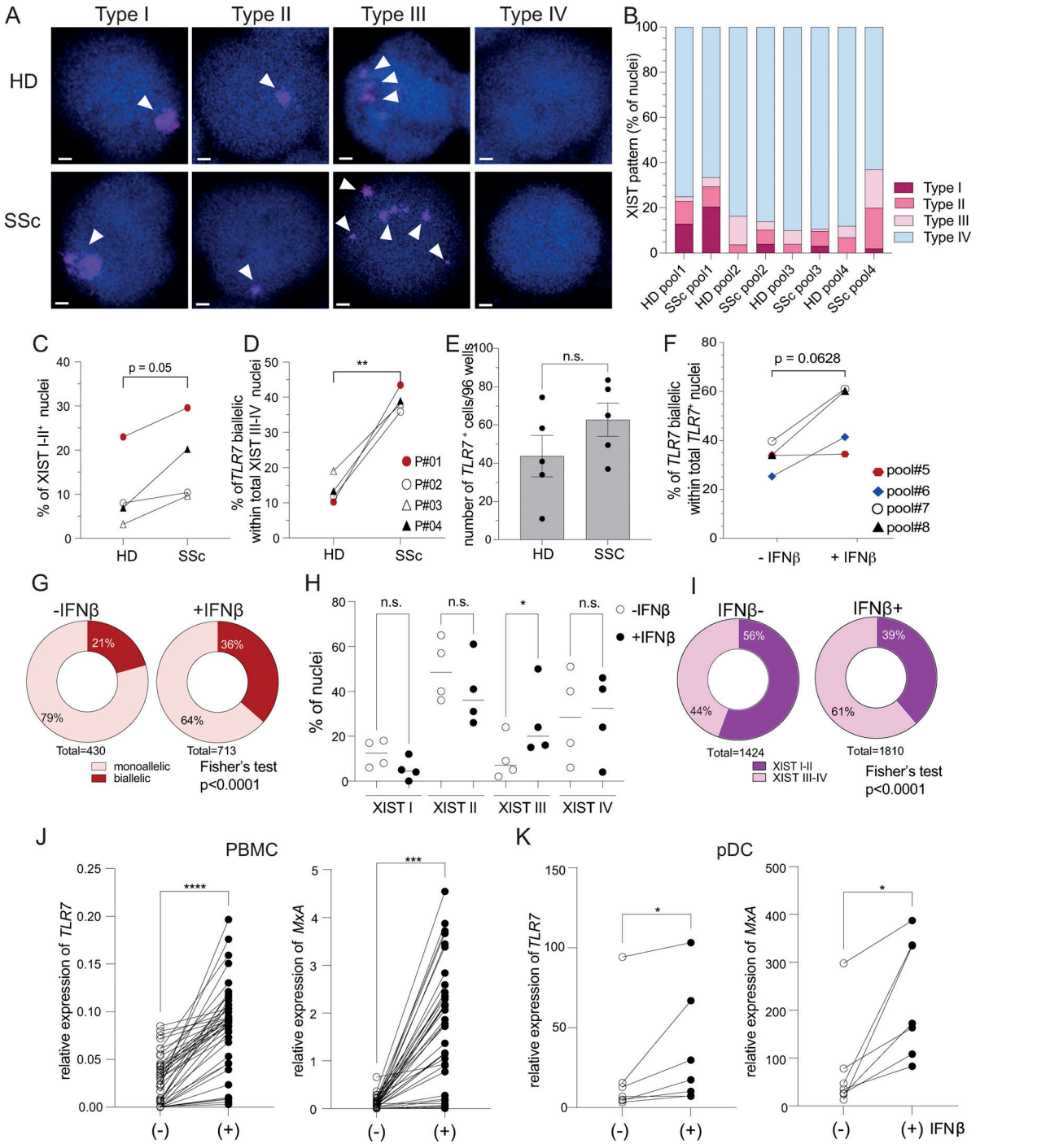

Figure S2. **XIST RNA localization profiles and impact of IFN-I signaling on XCI escape and expression levels of *TLR7* in female pDCs. (A)** RNA FISH representative images of *XIST* patterns I–IV from HD (upper panels) and SSc donors (lower panels). Arrowheads point to the different XIST patterns. Scale bars 1 µm. **(B)** Frequencies of XIST patterns, comparing HDs versus SSc pooled patients in four independent experiments (P#01 to P#04). **(C and D)** Graphs representing the frequencies among (C) the I and II XIST patterns, and (D) the frequencies of *TLR7* biallelic nuclei among pDCs with Type-III and -IV XIST patterns in paired experiments (n = 4). Statistical differences were analyzed using a paired Student's t test. **(E)** mRNA *TLR7* positive cells in 96-wells plate from HDs (n = 5) and SSc donors (n = 5). Statistical analysis was performed using a Mann–Whitney test. **(F)** Frequencies of *TLR7* biallelic cells, relative to the total *TLR7*$^+$ nuclei in IL-3-pDCs stimulated or not with IFN-β for 2 h before RNA-FISH (n = 4, pool#5 to #8). **(G)** Frequencies of *TLR7* biallelic nuclei among total nuclei counted from all the pooled donors IFNβ$^-$ (n = 430) and IFNβ$^+$ (n = 713). Statistical differences were analyzed using a Fisher's exact test. **(H)** Frequencies of XIST patterns I–IV comparing cells incubated in medium (–IFN-β) or with IFN-β (n = 4, pool#5 to #8). Statistical analysis performed with a repeated measured one-way ANOVA test. **(I)** Frequencies of nuclei with XIST Type-I and -II pattern calculated from the total nuclei from all pooled donors, with Medium (IFNβ$^-$; n = 1,424) and IFNβ$^+$ (n = 1,810). Statistical analysis was performed using a Fisher exact test. **(J)** mRNA was isolated from 41 PBMCs samples incubated or not with IFN-β (1 ng/ml) for 3 h. *TLR7* and *MxA* gene expression was analyzed by RT-qPCR and normalized over GAPDH expression. **(K)** mRNA was isolated from purified pDCs incubated or not with IFN-β (1 ng/ml) for 3 h. *TLR7* and *MxA* gene expression was analyzed by RT-qPCR and normalized over GAPDH expression. Statistical analyses were performed with a Wilcoxon test (J) and a Student's paired t test (K). *P < 0.05; **P < 0.01; ***P < 0.001.

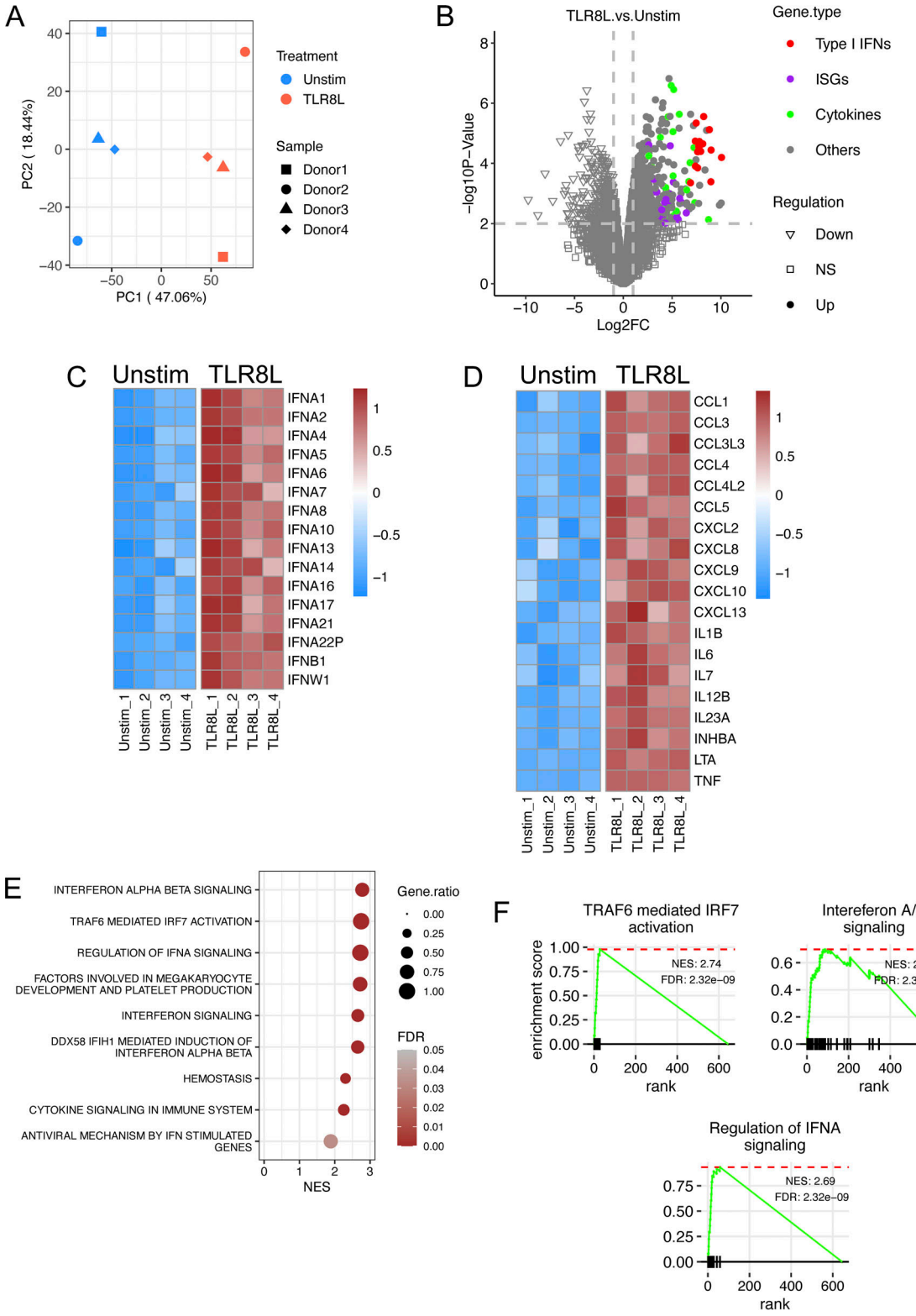

Figure S3. **TLR8 signaling induces inflammatory cytokines and IFN-I–driven response in pDCs of patients with SSc. (A–F)** Purified pDCs from SSc patients (n = 4) were stimulated with ORN-8L, or left Unstim for 6 h. The RNA was harvested for RNA-seq. **(A)** PCA of transcriptome in Unstim or TLR8L-stimulated SSc pDCs. **(B)** Volcano plot comparing gene expression between TLR8L-stimulated and Unstim SSc pDCs. IFN-Is, ISGs, cytokines, and other up-regulated genes are labeled in red, purple, green, and grey, respectively. Genes with down-, not significant (NS), and upregulation are shaped by a triangle, square, and circle, respectively. **(C and D)** Heatmap (LogCPM) comparing TLR8L-stimulated and Unstim SSc pDCs of differentially expressed (C) IFN-Is and (D) inflammatory cytokines with a threshold at $Log_2FC > 1$ and adjusted P value <0.05. **(E)** Gene set enrichment of Reactome subset of the MSigDB canonical pathways collection of differentially expressed genes of TLR8L versus Unstim condition. **(F)** Gene set enrichment analysis of genes correlated with top three upregulated pathways by TLR8L stimulation.

Provided online are Table S1, Table S2, Table S3, and Table S4. Table S1 shows design of the experimental PBMC pools from SSc and HD tested for pDC enrichment and RNA FISH analysis. Table S2 shows clinical and demographic characteristics of the SSc patients (U.S. cohort). Table S3 shows clinical and demographic characteristics of the SSc patients (France cohort). Table S4 shows clinical and demographic characteristics of the SSc patients used for scRNA-seq analysis.